# Virginia Tech Morphing Wing Team
# Spring 2005 Final Report

**Desta Alemayehu**
**Mathieu Leng**
**Ryan McNulty**
**Michael Mulloy**
**Ryan Somero**
**Cyril de Tenorio**
**Aerospace and Mechanical Engineering Departments**
**Virginia Tech**
**May 11, 2005**

## Table of Contents

# 1. Introduction

## 1.1 Why Morph

It has always been the goal of aerospace engineers to design planes that fly faster, further, and higher. With today's technology we are able to fly faster than ten times the speed of sound, around the world without refueling, and over 350,000 feet high, but none of these planes could do all three. With every design come tradeoffs between the different flight regimes. Traditional fixed wing geometry aircraft are designed to efficiently fly within one flight regime. Morphing wing technology, however, has begun to break down the barriers of tradeoffs.

## 1.2 History of Morphing Technology

On June 10, 1951, the X-5 by Bell Aircraft became the world's first aircraft to sweep back its wings during flight. The X-5 was built to demonstrate the ability to sweep in flight angles of 20,45, and 60 degrees at subsonic and transonic speeds. The X-5's ability to successfully demonstrate this capability made way for the first military use of swept wings with Grumman Aircraft's F-10-F.[1]


[1]**Pilotfriend**. **"Variable Sweep Wings" Avail. http://www.pilotfriend.com/century-of-flight/index.htm**

The United States Navy today takes advantage of the ability to change the sweep angle with the F-14 Tomcat. The F-14's normal sweep range is from 20 to 68 degrees and is able to "oversweep" to 75 degrees. The slightly swept wing position is ideal of short take off and landings from carriers, as well as low speed and fuel-efficient flight. The fully swept back position is ideal for supersonic speeds, maneuverability, and aircraft

storage on the carrier. The ability to morph gives the F-14 the ability to fly at speeds up to Mach 1.88 and up to a range of 500 nautical miles.[2]

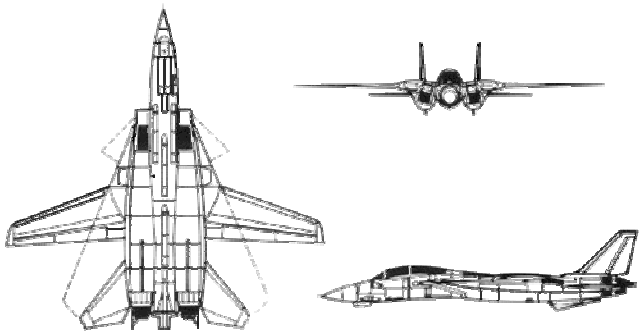

[2]**The Federation of American Scientists. "F-14 *Tomcat*" Avail. http://www.fas.org/man/dod-101/sys/ac/f-14.htm**

### 1.3 Morphing Aircraft of the Future

The Defense Advanced Research Projects Agency, DARPA, is working to develop an aircraft with the ability to morph in a far more dramatic fashion than currently possible. Lockheed Martin and NexGen Aeronautics have both developed an initial prototype for this project. Lockheed Martin's concept involves a folding wing technology, similar to that of a sea gull's wings. The wings fold up to the fuselage and are deployed for the full span condition.

**NewScientist.com.** "**The next 100 years of flight" Avail. http://www.newscientist.com/news/**

NexGen's concept uses a sliding skin technology. The use of sliding skin allows for sweep, chord, and span change without the heavy pin joints required with today's variable sweep fighters. Using the sliding skin technology, the air loads are distributed over a greater area, decreasing the necessary strength of joints and therefore decreasing the weight of those joints. The NexGen Concept is capable of optimizing performance for high speed flight, take off and landing, maneuvering, and loitering.

**(Image: NexGen)**

### 1.4 Last Semester's Achievements

The goals that were set for last semester on this design project were mainly made in preparation for this semester. Overall the team was testing concepts and ideas to see which would prove to be the best for our overall goal; flying a remote control airplane that morphs during flight. The morphing would involve changes that allow for four different wing configurations. These configurations are dash, loiter, landing, and maneuvering. Each configuration has an advantage to its design. With a morphing wing our airplane will be able to utilize all of these advantages based on what our mission is for the airplane, at that time.

Our team split up into two sub-groups with one half focusing on the morphing concepts, while the other half tested different airfoil shapes. The first groups main goal was to create a half span wing that had three different morphing characteristics. The three morphing characteristics that the team came up with is a change in span, a change in sweep angle, and a change in chord length. The purpose of making only a half span concept last semester with these morphing characteristics was not to see if they made big changes in performance, but to see if the three different wing changes could actually be housed structurally in the same wing. The purpose was to also prove that these concepts could actually work to change the wing shape.

Once the half span was constructed, it was to be tested in the Virginia Tech wind tunnel. The purpose of this was to make sure that all of the different morphing could take place while under an aerodynamic load. For this to be done a new test stand had to be constructed for the wind tunnel due to the large size of the half span. Once everything was built, the wing was placed in the wind tunnel and tested while under aerodynamic loads.

The results of this testing showed our team a lot of places that needed improvement. First, the sweep and the change in chord length didn't work when actuated by remote control. The main cause of this was due to undersized motors and too much

friction in certain areas. Although the group found many areas of improvement, the span actuation couldn't have worked better. With the flip of the control stick on the remote the span extends and retracts quickly and with ease.

The other half of the team dealt with the shape of the airfoil to be used. With the trailing edge of the wing extending to increase the size of the chord length, there was a small cusp that would form in the airfoil profile. Our team was unsure exactly how this cusp would affect the lift created by the wing, so different airfoil shapes were used to see which would perform the best in an extended and retracted configuration. To test to see which airfoil shape would perform the best, six foam models were bought from a foam cutting company. The total of six foam models came from three different airfoil shapes, each with two wing configurations; a retracted chord, and an extended chord. These foam models were also tested in the Virginia Tech wind tunnel to see which airfoil would perform the best in the extended and retracted configuration. Out of the three, the Clark-Y airfoil performed the best and is the shape we chose to go with for this semester's work.

### 1.5 This Semester's Goals

It is the goal of the 2004 Virginia Tech Morphing Wing team to develop and build a morphing wing capable of optimizing its performance in four flight regimes: Dash, Maneuver, Loiter, and Take-off / Landing.

The Dash regime is defined as a high-speed attack regime. It is configured for a low surface area, low span, and high sweep angle. This configuration produces low drag by having a streamlined profile as well as low induced drag.

The Loiter regime is defined for high endurance. It is configured to have a high aspect ratio and low sweep angle. The Loiter regime is designed to perform at minimum power and low speeds to allow for maximum time in the air.

The Maneuver regime is defined as a maximum control regime. It is configured for high lift capability and late and controlled stall. This regime experiences high structural loads due to the high load maneuvers.

The main goal for this semester was to make a remote control airplane whose wings morph in the three different aspects, as stated last semester. These three different morphs

will allow us to again achieve the four different wing configurations of dash, maneuver, loiter, and landing. The morphing aspects were a change in sweep angle, span length, and chord length. Using the knowledge we gained from last semester we were able to choose exactly how we were going to accomplish these goals.

For the sweep angle we needed to find a bigger motor with more torque while at the same time reducing the amount of friction in the power screw assembly. We also wanted to have our wing sweep back to an angle of 45 degrees, which is about 15 more degrees than last semester.

Our group was very pleased with how the span extension worked last semester so we decided to keep the actuation the same. For the actual extension itself though, our team wanted to make a more significant increase in span. We wanted to do this so that there would be more of an increase in performance during a loiter configuration.

Lastly our team wanted to simplify the chord extension. Due to structural issues and actuation problems last semester, we decided to change the chord extension to a slotted fowler flap. This would allow our airplane to still have an increase in chord length while also getting a lot better performance than our chord extension did last semester. With these changes from last semester our team was still able to meet the goal of making a morphing wing that can meet the four wing configurations for loiter, dash, maneuvering, and landing.

# 2. Aircraft sizing and geometry selection

### 2.1 Data Collection

The characteristics of several existing model airplanes have been collected to serve as a guide for the initial sizing of the VT Morphing aircraft.

**Table 2.1.** Characteristics of model airplanes.

| MODEL AIRPLANE | ENGINE SIZE (*cu in)* | WEIGHT *(W, lbs)* | WING AREA (S, $in^2$) | WING SPAN (b, *in)* | ASPECT RATIO (AR) | WING LOADING (lbs/ $ft^2$) | FUSELAGE LENGTH ($L_F$, in) |
|---|---|---|---|---|---|---|---|
| Top Flite P-51D Mustang Giant Gold Ed Kit 2.1-2.8,84.5" | 2.8 | 23 | 1245 | 84.5 | 5.7 | 2.7 | 73.5 |
| Top Flite P-47D Thunderbolt GSGE Kit 2.1-2.8,85" | 2.8 | 22 | 1327 | 85 | 5.4 | 2.4 | 75.5 |
| Top Flite F4U Corsair GSGE Kit 2.1-2.8,86.5" | 2.8 | 26 | 1344.5 | 86.5 | 5.6 | 2.8 | 77.5 |
| Midwest North American AT-6 Kit .90-1.20,83" | 1.2 | 15 | 1000 | 83 | 6.9 | 2.2 | 55.5 |
| Top Flite AT6 Texan Gold Edition .61-.90,69.4" | 0.9 | 10 | 713 | 69.4 | 6.8 | 2.0 | 53 |
| Top Flite P-51D Mustang Gold Edition Kit .60-.90,65" | 0.9 | 10 | 734 | 65 | 5.8 | 2.0 | 56.5 |
| Top Flite F4U Corsair Gold Edition Kit .60-.80,62" | 0.8 | 9.5 | 700 | 62 | 5.5 | 2.0 | 48.5 |
| Top Flite P-47D Thunderbolt Gold Edition Kit .61-90,63" | 0.9 | 10 | 713 | 63 | 5.6 | 2.0 | 55 |
| House Of Balsa T-6 Texan Kit .15-.19,44" | 0.19 | 3 | 319 | 44 | 6.1 | 1.4 | 29.3 |
| Great Planes P-51D Mustang 40 Kit .40-.46,57" | 0.46 | 6 | 580 | 57 | 5.6 | 1.5 | 50 |
| Great Planes F4U Corsair 40 Kit .40-.46,56" | 0.46 | 6 | 573 | 56 | 5.5 | 1.5 | 43 |
| Great Planes Extra 300S 40 Kit .40-.51,58" | 0.51 | 5.75 | 594 | 58 | 5.7 | 1.4 | 48 |
| Tower Hobbies Tower Trainer 60 MKII ARF .46-.61,69.5" | 0.61 | 7.5 | 877 | 69.5 | 5.5 | 1.2 | 57.25 |
| Hobbico Hobbistar 60 MK.III ARF .61,71" | 0.61 | 7 | 887.5 | 71 | 5.7 | 1.1 | 55 |
| Goldberg Protege 60 Kit .40-.60,71.5" | 0.6 | 7.75 | 860 | 71.5 | 5.9 | 1.3 | 56 |
| Great Planes ElectriFly PT-Electric Trainer Kit | N/A | 2.75 | 500 | 56 | 6.3 | 0.8 | 39.5 |

| | | | | | | | |
|---|---|---|---|---|---|---|---|
| Great Planes Spirit 100 Kit 99.5" | N/A | 4.06 | 946 | 99.5 | 10.5 | 0.618 | 51.5 |
| Great Planes Spirit Elite 2-Meter Kit 78.5" | N/A | 2.1875 | 645 | 78.5 | 9.6 | 0.488 | 46 |
| Great Planes ElectriFly Spectra Kit 78.5" | N/A | 3.00 | 676 | 78.5 | 9.1 | 0.639 | 38 |
| Great Planes Spirit 2-Meter Kit 78.5" | N/A | 1.875 | 676 | 78.5 | 9.1 | 0.399 | 39.25 |

### 2.2 Weight Estimation

Initial weight estimation for the proposed design was conduction for two reasons. First, the weight estimation was required to size the main wing and wing extensions. Second, it was used to determine weather the engine selected for this design would provide adequate power.

The first step in conducting the weight estimation was to divide the aircraft into seven components. The seven components, which made up the aircraft, were propulsion, landing gear, fuselage and tail, wings, actuation systems, radio control, and payload. Then the weight of each component was determined by summing the weight of each part, which made up that component. The detail of the weight estimation for each component is presented in Appendix B-1 (Tables B-1 through B-6). Table 2.1 below shows the resulting weight estimation for the complete aircraft.

**Table 2.2.** Complete aircraft weight estimation

| | |
|---|---|
| TOTAL (ozs) | 238.6 |
| (lbs) | 14.91 |

| PART | COMPONENT WEIGHT, oz | COMPONENT WEIGHT, lbs |
|---|---|---|
| Propulsion | 58.4 | 3.65 |
| Wing | 58.0 | 3.63 |
| Fuselage and tail | 25.0 | 1.56 |
| Actuation system | 24.5 | 1.53 |
| Radio control | 18.2 | 1.13 |
| Landing gear | 22.5 | 1.41 |
| Payload | 32.0 | 2.0 |

### 2.3 Engine Sizing

To size the engine, the team first evaluated one that was currently available. This latter, the O.S. 0.91 FX glow engine, has an operating range for an aircraft weighting between 10 to 12 pounds. As presented in the previous section, the weight of the VT Morphing aircraft was estimated to 14.91 lbs. This estimation being very conservative and only slightly overweight for this engine, the team decided that it was not reasonable to invest in new engine. The following figure shows a plot of engine size versus weight for the airplane models presented in Table 2.3.

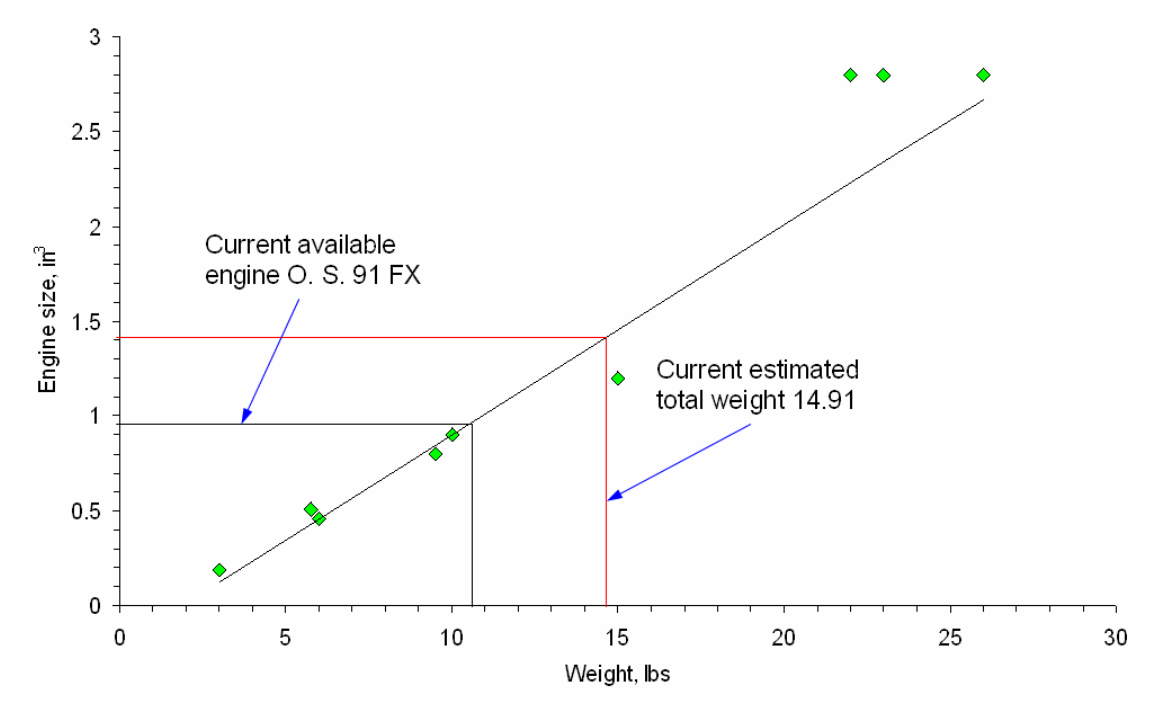


**Figure 2.3** Comparative plot of engine size versus weight for several scales model

To achieve a similar performance as the scale model planes used in the above plot, an O.S.1.4 engine would be ideal. However, all glow engines are usually overpowered, so the O.S. 0.91 FX glow engine can be used with reduced performance. A schematic of the engine is shown in Figure 2.2 and Table 2.3 lists its specifications.

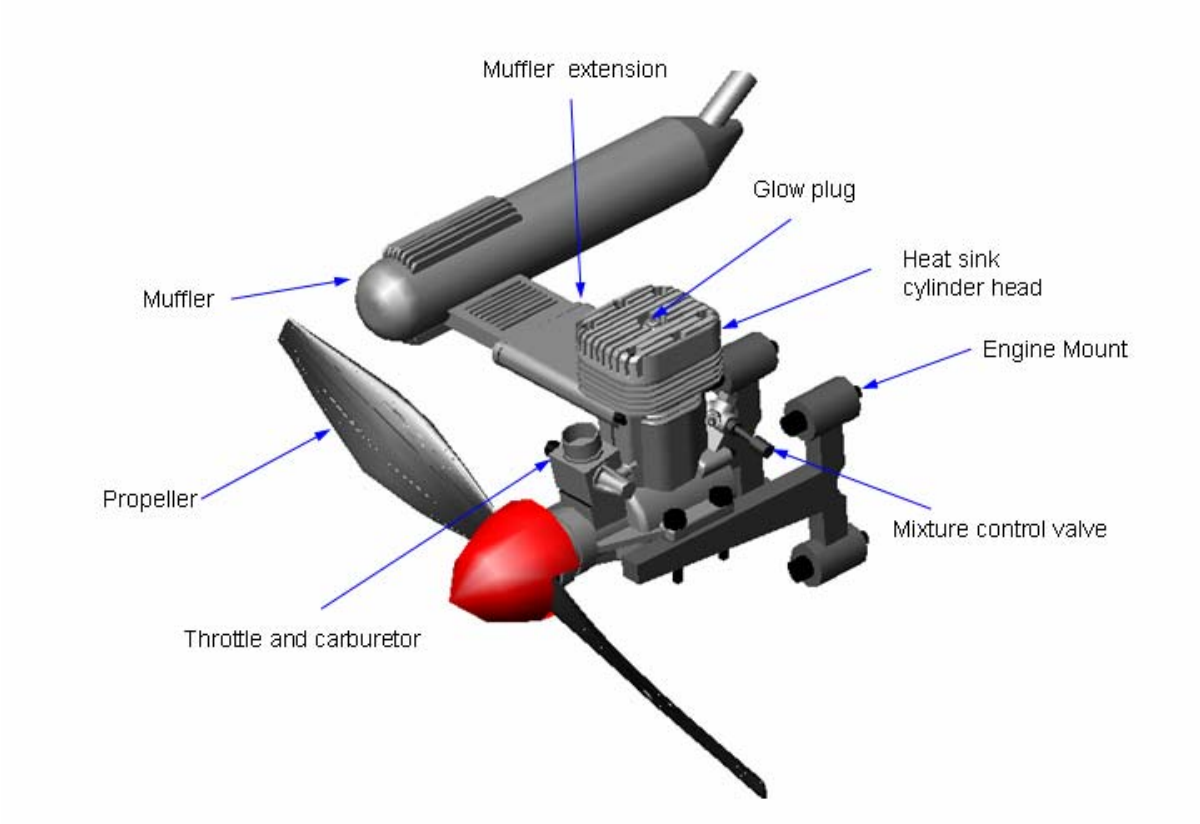


**Figure 2.2** Schematic of the O.S. 0.91 FX engine.

**Table 2.3.** Specification of the O.S. 0.91 FX engine

| | |
|---|---|
| Displacement | 14.95cc (0.912 cu in) |
| RPM range | 2,000 - 16,000 |
| Bore | 27.7mm (1.090") |
| Stroke | 24.8mm (0.976") |
| Compression Ratio | 10.1 : 1 |
| Weight | 550g (19.42oz)  24.3 oz w/muffler |
| Horsepower | 2.8 BHP at 15,000 RPM |
| Length | 96mm the distance from the back plate to drive washer |
| Height | 103mm |
| Width | 42.6mm width of engine neglecting engine mounting flanges52.0mm distance between centers of the mounting holes |
| Crankshaft Thread Size | 5/16-24 |

## 2.4 Wing airfoil section and geometry selection

The airfoil selection was based on a compromise between aerodynamic performance and practicality of the construction. The Clark-Y airfoil, so named after its designer, Col. Virginius E. Clark., was chosen because it has a flat lower surface from 30% chord to the trailing edge, which facilitates the construction of the wing. Moreover, this airfoil has been proven to be reliable as it is widely used for model airplanes. Figure 2.3 shows the Clark-Y airfoil profile. The corresponding tabulated coordinates are presented in Appendix B-.2 (Table B-7). The geometric and 2-D aerodynamic characteristics of the Clark-Y are also presented in appendix B-2.

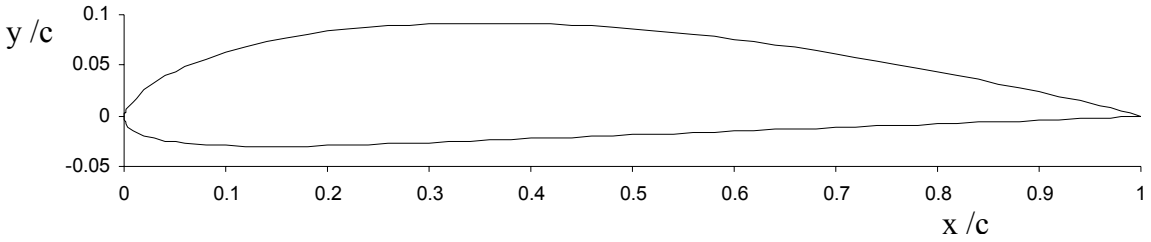


**Figure 2.3** Clark Y airfoil shape

Also for practical purposes, the simplest possible wing geometry was selected, namely a standard rectangular, untapered wing with neither dihedral nor twist.

## 2.5 Wing Sizing

The main goal driving the wing sizing was to obtain considerable changes in shape between the different configurations of the VT Morphing aircraft while ensuring good aerodynamic performances.

### 2.5.1 Main wing sizing

The unswept retracted wing configuration of the VT Morphing aircraft corresponds primarily to take-off and landing. No specific landing distance being stated as a requirement, the main wing was sized based on take-off performance. One of the major advantages of the morphing airplane is that it has room for adjustments. For instance, part of the span-extension can be used for landing if necessary. The lift-off speed equation is:

$$V_{LO} = 1.2\, V_{stall} = 1.2\sqrt{\frac{2W}{\rho_\infty S C_{L,\max}}} \qquad (2.1)$$

where the factor of safety of 1.2 corresponds to a $V_{LO}$ 20% higher than $V_{stall}$

The requirement for the main wing sizing was to achieve a take-off speed in the range of 30 to 35 mph. Recall that the take-off weight was estimated as $W$ = 14.91 lb. As shown on Figure B-1 (appendix), the 2-D maximum lift coefficient for the Clark-Y airfoil is about 1.4 for such a speed range (corresponding to Reynolds number in the range of 250,000 to 350,000). According to existing data (Ref.2.1) and wind tunnel data acquired in the fall semester (Ref.2.2), 3-D effects reduces the $C_{L,max}$ of the Clark-Y to about 1.2 or 1.1 for a rectangular wing with an aspect ratio in the range of 5 to 6 and at a Reynolds number in the range of 200,000 to 1,000,000. With a very conservative estimation of the gain in maximum lift coefficient ($\Delta C_{L,max}$) due to flap effects of 0.2, the $C_{L,max}$ for take-off was fixed as 1.3 in equation (2.1).

Based on the characteristics of other model airplanes (Table 2.1), the wing loading (W/S) was limited to 2.6. Although this value may appear high, the wing loading at take-off will be the maximum of any configuration of the aircraft since it is the one with the smallest surface area. Another self-specified requirement was to have a wing aspect ratio in the range of 5 to 6 for this configuration. This range was chosen to match those of general aviation and trainer model airplanes while leaving room for a substantial increase for the loiter configuration. For the latter reason and for construction space constraint, it was also decided to keep the main wing span under 6 feet.

The following constraint plot was used to determine the chord and span of the main wing that satisfy the aforementioned requirements:

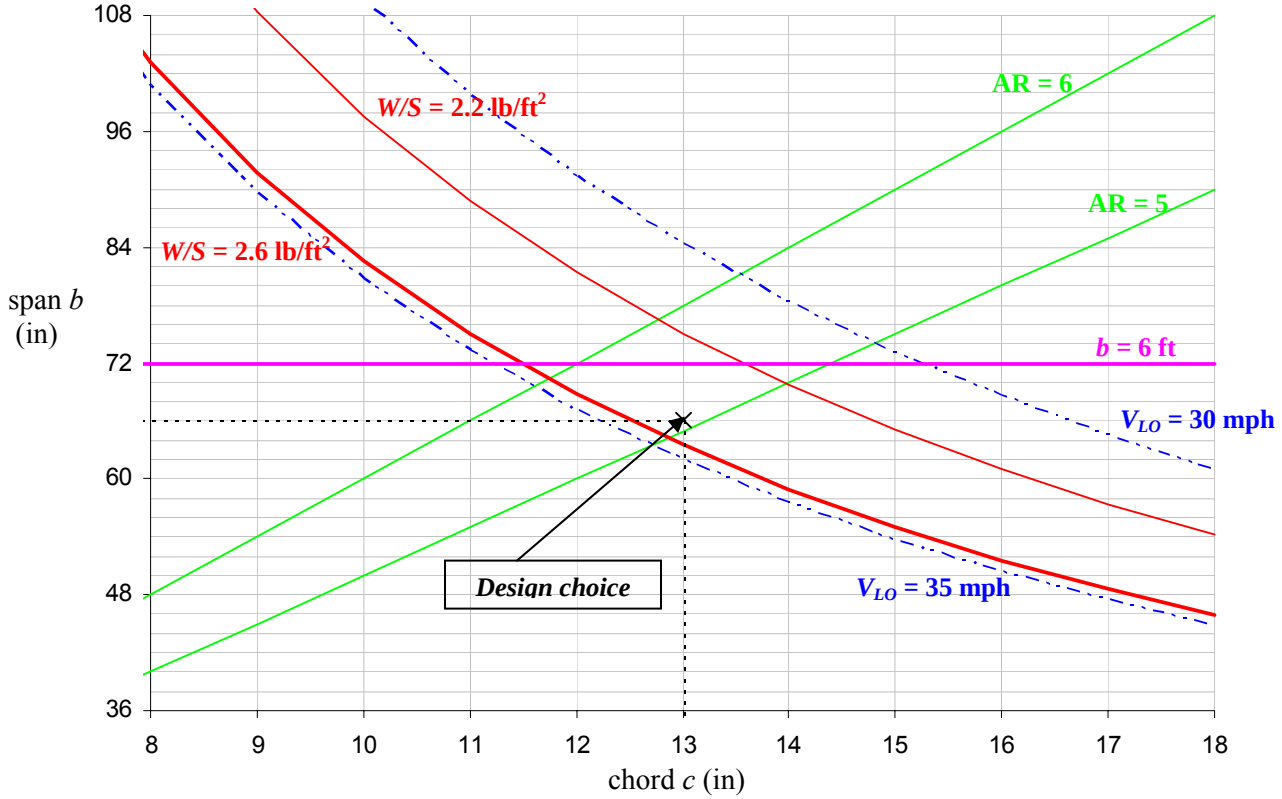


**Figure 2.4** Constraint plot used to determine the chord and span of the main wing.

As shown on the above figure, a narrowed design space was obtained and the values of 13 inches and 66 inches (5.5 ft) were selected for the chord and span of the main wing, respectively. These values corresponds to a lift-off speed velocity $V_{LO}$ = 33.9 mph, an aspect ratio $AR$ = 5.08 and a wing loading $W/S$ = 2.5 lb/ft$^2$.

### 2.5.2 Span-extensions sizing

The main goal driving the sizing of the wing-extensions was to obtain considerable changes in shape between the retracted and extended configuration of the wing. The major constraint was on the extension chord $c_e$, limited to 8.625" (about 66% of the wing chord $c$) by the space necessary for ailerons, flaps, and structure of the main wing. The team decided to aim for an aspect ratio of 9 for the extended-span configuration in order to match the characteristics of glider airplanes (see last 4 rows of Table 2.1). The fraction of span increase $x$ required to achieve an aspect ratio of 9 was determined using the equation for the aspect ratio of the wing in this "loiter" configuration is:

$$AR_l = \frac{b_l^2}{S_l} = \frac{[(1+x)b]^2}{bc + xb(0.66c)} \quad \Rightarrow \quad \frac{(1+x)^2}{1+0.66x} = \frac{AR_l}{AR} \tag{2.2}$$

Solving the above equation for $x$ with $AR_l/AR = 9/5.08$ gives $x \approx 0.56$. This value corresponds to a wing span $b_l = 103$ inches (8'7"), which produces a span increase of 56 % and an aspect ratio increase of 77 %.

Finally, space was required in the main wing for actuation. In addition, a portion of the extension needs to stay in the main wing in the fully extended configuration. As a result, the dimensions of the extensions were set as $c_e = 8.625$ in and $b_e = 21$ in. When fully extended, each extension will be 18.5" out of the main wing while 2.5" will stay inside. Thus, with the extension fully retracted, there will remain 4" of free space for actuations. This is illustrated by the following figure:

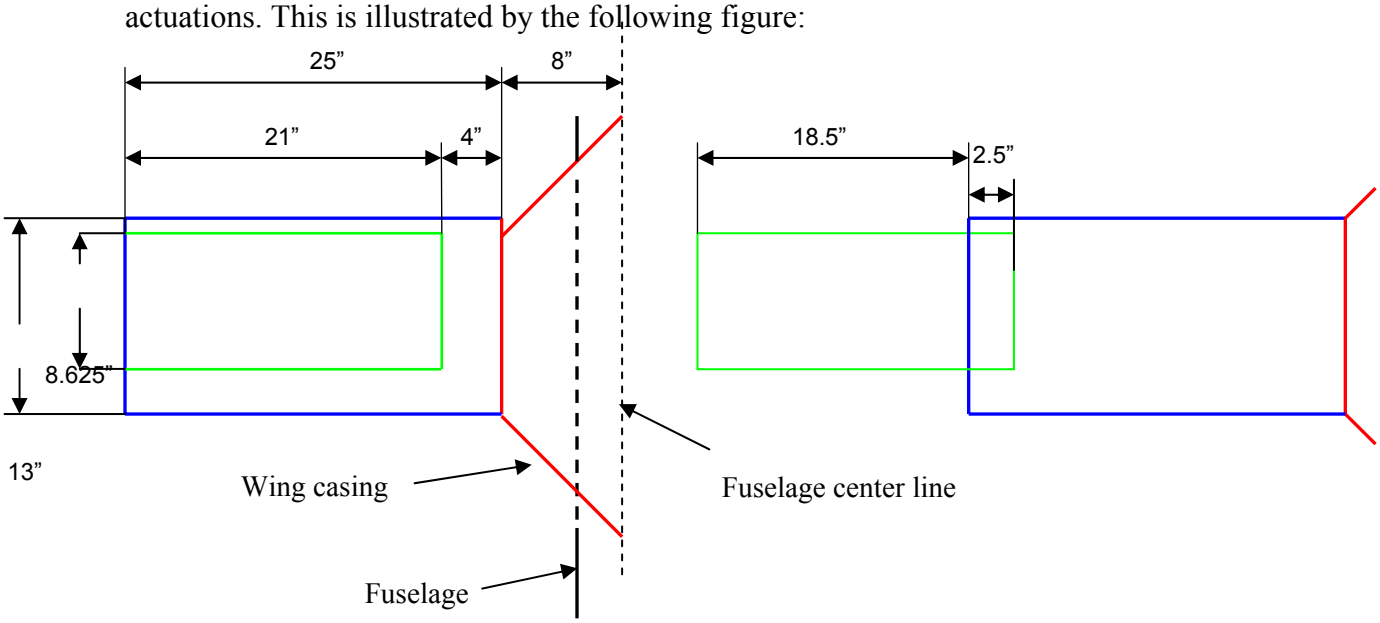


**Figure 2.5** Schematic illustrating the main wing and span-extension dimensions

The resulting wing characteristics are presented by the following table:

**Table 2.4.** Geometric properties of the wing.

| | Wing Area $S$ (in$^2$) | Span $b$ (in) | Mean Geometric Chord $c'$ (in) | Aspect Ratio $AR$ | Mean Aerodynamic Chord $\bar{c}$ (in) |
|---|---|---|---|---|---|
| Span-extension fully in | 858 | 66 | 13 | 5.08 | 13 |
| Span-extension fully out | 1177.1 | 103 | 11.43 | 9.01 | 11.81 |

The mean geometric chord and mean aerodynamic chord were computed according to the following definitions (from Ref.3.4):

$$c' = \frac{2}{b}\int_0^{\frac{b}{2}} c(y)dy = \frac{S}{b} \tag{2.3}$$

$$\bar{c} = \frac{2}{S}\int_0^{\frac{b}{2}} c(y)^2 dy \tag{2.4}$$

The wing casing shown on Figure 3.5 was required to implement the variable sweep ability of the VT Morphing aircraft. It is an open structure sitting on top of the fuselage that allows the wing to rotate in and out. The reasons for its shape and dimensions are presented in the next section.

## 2.6 Wing Sweep

### 2.6.1 Purpose

The primary purpose of wing sweep is to reduce the adverse effects of shock waves formation on the wing in transonic and supersonic flight. It is thus not relevant to the VT morphing aircraft since it is a model airplane that will never be even close to reach transonic speed. However, wing sweep was incorporated to the design because it was a

major requirement of the project. Indeed, the VT morphing aircraft must be capable of considerable changes in shape and specifically must be able to morph into a "Dash" configuration, which requires sweeping of the wing. The team decided to aim for a 45 degrees maximum sweep, which gives a sweep range of 0 to 45 degrees close to current variable sweep military aircrafts. For instance, the F-111 Aardvark has wings angle from 16 (full forward) to 72.5 degrees (full aft) and the F-14 Tomcat has a normal sweep range of 20 to 68 degrees.

### 2.6.2 Expected effects of variable sweep

The design challenge generated by using variable sweep is to control the movements of the aerodynamic center and center of gravity that go along with the sweep of the wing. According to Raymer (Ref. 2.3), when the wing swings aft, both the aerodynamic center and the center of gravity move with it, but the latter not nearly as much as the first. As a result we expect the static margin to increase as the wing sweeps back. For an aircraft, the stick-fixed static margin is defined as (from Ref. 2.4):

$$K_n = h_n - h = \frac{x_{ac}}{\bar{c}} - \frac{x_{cg}}{\bar{c}} \qquad (2.5)$$

A positive static margin is a required condition for longitudinal static stability. Therefore, as the wing sweeps back, the aircraft is expected to become more and more stable, and possibly too stable. The common way to counteract this effect is to move mass inside the airplane (usually fuel) to create an additional backward shift of the center of gravity. The other option to balance the aircraft is to have a tail providing a tremendous down-load. The latter solution was chosen to balance the VT Morphing aircraft. Indeed from computational stability analysis (using the numerical code VLMpc), the maximum static margin, occurring when the wing is fully swept (45º), was estimated to be about 35 %. This value being not excessively high, a system of moving masses inside the aircraft was not considered indispensable. Moreover such a system would have added undesired complications and weight to the design. Therefore, the tail was designed such as to ensure the required countermoment to balance the aircraft in its fully swept configuration. The details of the stability analysis using VLMpc are presented in the Aerodynamic section (section 6) of this paper.

### 2.6.3 Pivot point location

According to Ref. 2.3, the pivot position about which the wing is swept must be near the thickest part of the chord, usually between about 30 and 40 % of the chord distant from the leading edge of the wing. For the Clark-Y airfoil, the maximum thickness is located at 29 % of the chord. However, for practical purposes, the team decided to position the pivot point aligned with the spar of the wing, which is at 25 % of the chord, approximate location of the aerodynamic center of the wing.

The longitudinal location of the pivot point being fixed, all that needed to be determined was its lateral position. This was done so that when fully swept, the wing would have its leading edge perfectly aligned with the leading edge of the wing casing. The pivot position was thus obtained through simple geometry as illustrated by the following figure:

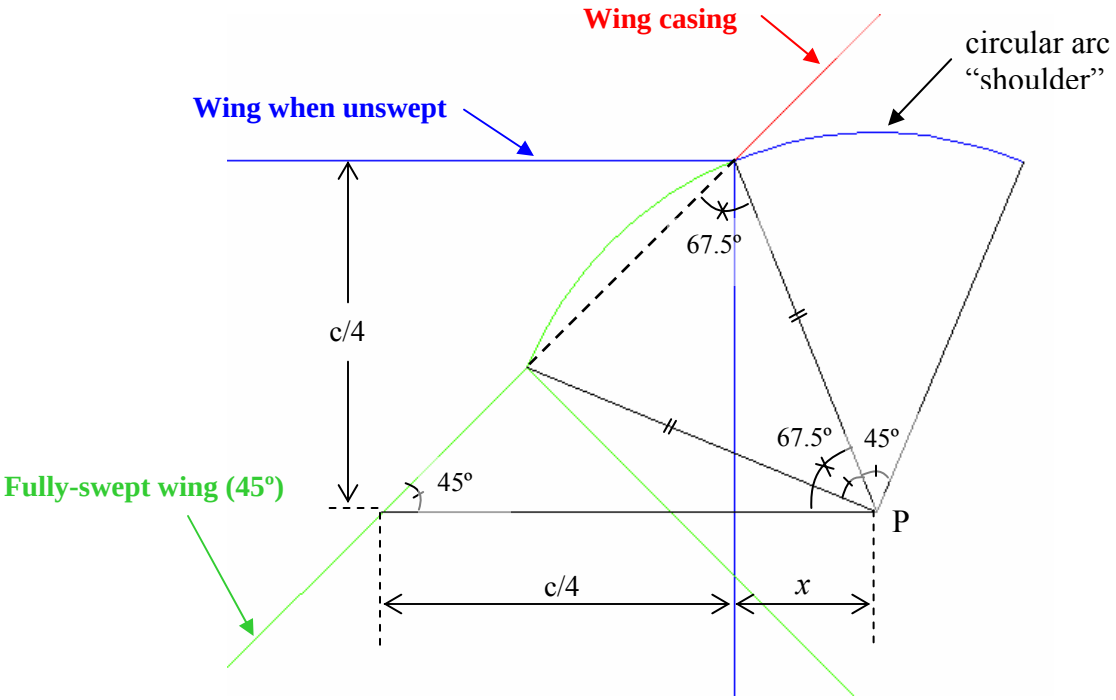


**Figure 2.6** Sketch illustrating the pivot position calculation

The distance $x$ shown on the above figure between the pivot point and the root chord of the wing when unswept was computed as:

$$x = \frac{c/4}{\tan(67.5°)} = \frac{(13\,in)/4}{\tan(67.5°)} \quad \Rightarrow \quad x = 1.346\ inches \tag{2.6}$$

As illustrated by Figure 3.6, in order to avoid any gap between the casing and the wing when the latter sweeps back, a component must be added to the wing at the root near the leading edge. This component must have a specific outer shape, namely a circular arc centered at the pivot point. Such a "shoulder" is commonly used by aircrafts with variable sweep, as for instance the F-14:

**Figure 2.7** Picture illustrating the "shoulder" on the F-14 (from sky-fly.com)

The pivot position being determined, the required casing width was computed also from simple geometry. When the wing sweeps to the maximum value of 45º, it was found that the wing root trailing edge moves inward by a lateral distance d = 7.289 in, as illustrated on the figure below. Therefore the team opted for a wing casing width of 16 inches.

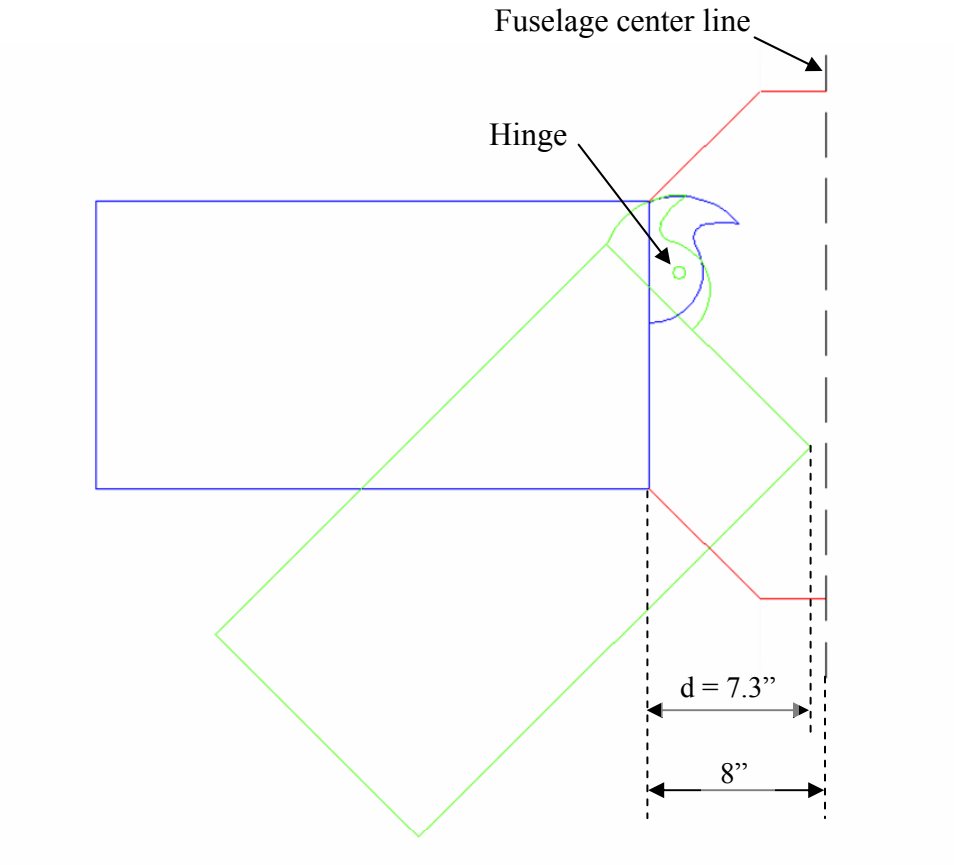


**Figure 2.8** Schematic illustrating the casing width required.

## 2.7 Fuselage

An initial fuselage estimation was made using statistical equations given by Ref. 2.3 which are based on historical data. However, the value obtained was unrealistically high for a model airplane. As a result, the first initial estimation was taken as 56 inches to match the fuselage length of the *Midwest North American AT-6 Kit .90-1.20,83"* model airplane (4$^{th}$ row in Table 2.1). Indeed, this scaled model exhibits characteristics very similar to the VT morphing airplane: it has nearly the same weight and has wing dimensions in between the span-retracted and span-extended configurations of the VT morphing. The first estimations was then refined when the tail was sized, as it is explained in the next section. The final required fuselage length obtained after analysis was 62.5 inches (as illustrated on figure 2.11). More details about the structure and dimensions of the fuselage are presented in the Fuselage Structure section (section 4.2).

## 2.8 Tail

### 2.8.1 Airfoil and Geometry selection

The tail arrangement chosen for the VT Morphing aircraft is the conventional tail, which is used by about 70% of the aircrafts and has thus been proven to work.

Concerning the airfoil selection, a NACA 0012 was chosen for the horizontal tail. This is a symmetric airfoil commonly used for this purpose. On the other hand, the team decided to use a flat surface for the vertical tail for practical purposes concerning the construction.

The choice of tail geometry was based on the following typical values of tail aspect ratio and taper ratio presented by Ref.2.3:

**Table 2.5.** Typical range for tail aspect ratio and taper ratio

| | Aspect ratio AR | Taper ratio $\lambda$ |
|---|---|---|
| Horizontal tail | 3-5 | 0.3-0.6 |
| Vertical tail | 1.3-2.0 | 0.3-0.6 |

The team decided to go with $AR_{HT} = 4$, $\lambda_{HT} = 0.6$ for the horizontal tail, and $AR_{VT} = 1.6$, $\lambda_{VT} = 0.5$ for the vertical tail.

### 2.8.2 Tail sizing

An initial estimation of the tail size was obtained using the “tail volume coefficient” method given by Raymer (Ref.2.3).

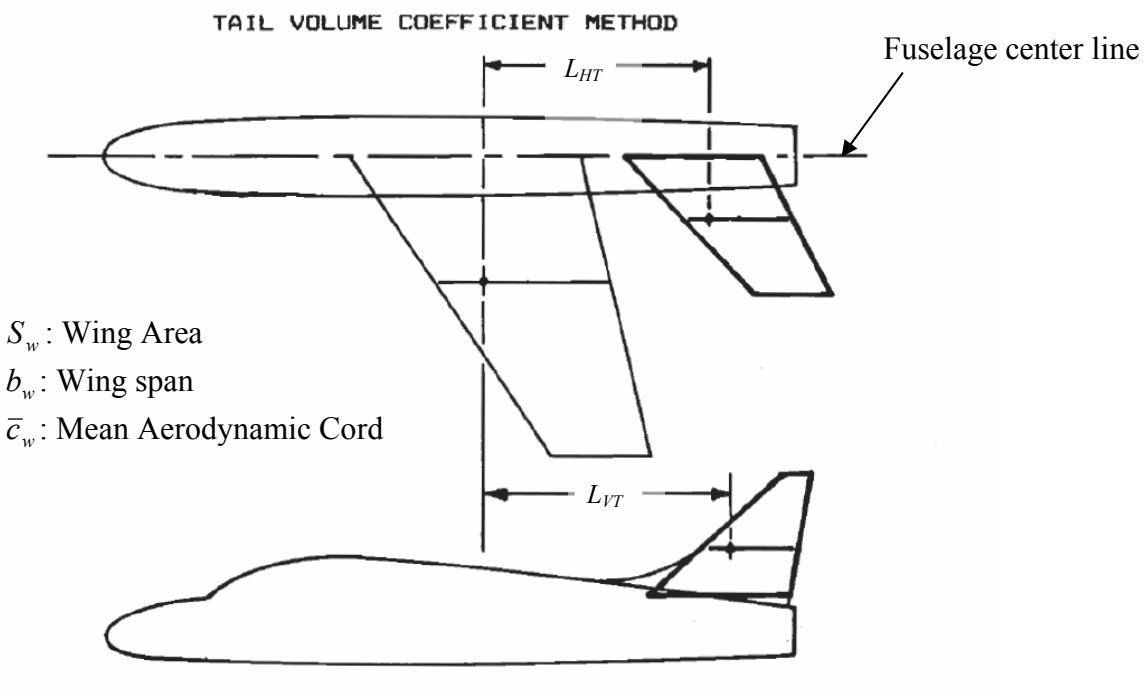


**Figure 2.9** Sketch defining the parameters used for initial tail sizing (from Ref.2.3)

The tail area was calculated using the following equation:

$$S_{VT} = c_{VT} b_w S_w / L_{VT} \tag{2.7}$$

$$S_{HT} = c_{HT} \bar{c}_w S_w / L_{HT} \tag{2.8}$$

Ref.3.3 presents typical values for the volume coefficients based on existing data for different classes of aircraft. The values given for general-aviation – single engine type of airplane were used, namely $c_{HT} = 0.7$ and $c_{VT} = 0.04$.

According to Ref.3.3, for an aircraft with a front-mounted propeller engine, the tail arm should be about 60% of the fuselage length. The fuselage length of the VT Morphing was first estimated as 56 inches, which results in a tail moment arm of $L_{HT} = L_{VT} = 33.6$ in.

Plugging back these numbers into equations (2.7) and (2.8) gave the following initial estimations for horizontal and vertical tail surface areas:

$$S_{HT} = 289.7 \text{ in}^2 \quad \text{and} \quad S_{VT} = 144.3 \text{ in}^2$$

It must be noted that when using equations (2.7) and (2.8), the wing span and wing area have been taken as their maximum possible values: respectively $b_w = 103$ in and $S_w = 1177.1$ in$^2$ which correspond to the unswept, span-extended configuration (loiter) of the VT morphing aircraft. Also, the value of the wing mean aerodynamic chord used was the one for loiter, namely $\bar{c}_w = 11.81$ in. Considering the span-retracted or swept

configuration would have resulted in smaller tail areas. The obtained dimensions are thus conservative estimations that will secure the complete flight envelope. However, results from stability analysis required an increase of the tail moment arm to counteract the effects of wing sweep discussed in the previous section. Indeed, as the wing sweeps back, the aerodynamic center of the wing also moves back, which decreases the tail moment arm $L_{HT}$. From numerical simulations using VLMpc, the backward shift of the aerodynamic center of the airplane was estimated to about 5.5 inches. This increment was added to the original moment arm value (33.6 in). As a result, the distance between the leading edge of the main wing and the leading edge of the horizontal tail, which is slightly bigger than the tail moment arm $L_{HT}$, was fixed as 40 inches. The tail dimensions were also refined by stability analysis. The final tail and fuselage dimensions determined after numerical simulations with VLMpc are shown on the following figures. The details of the stability analysis using VLMpc are presented in the Aerodynamic section (section 5) of this paper.

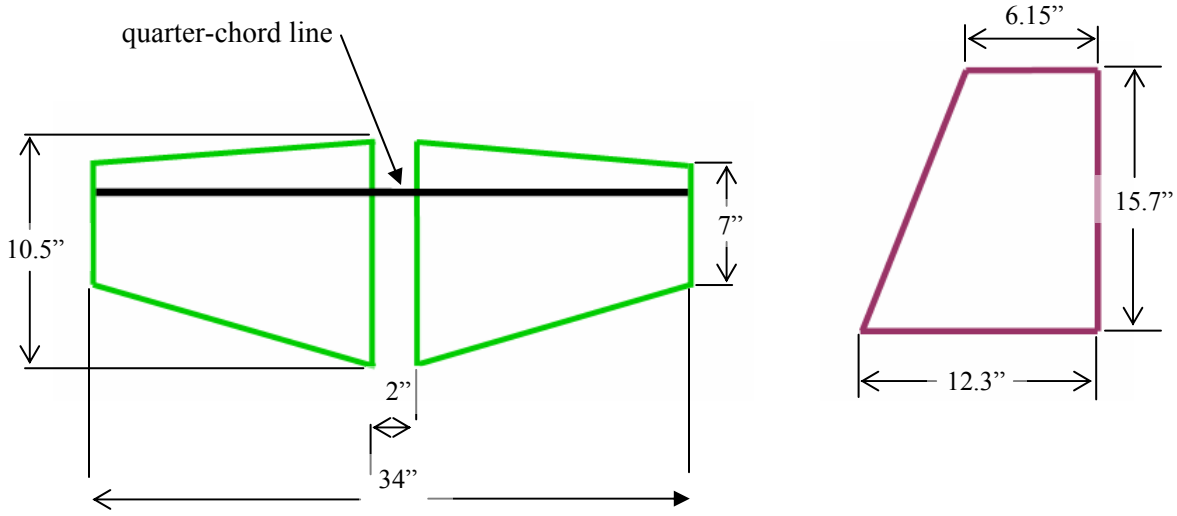


**Figure 2.10** Schematic illustrating the final tail dimensions

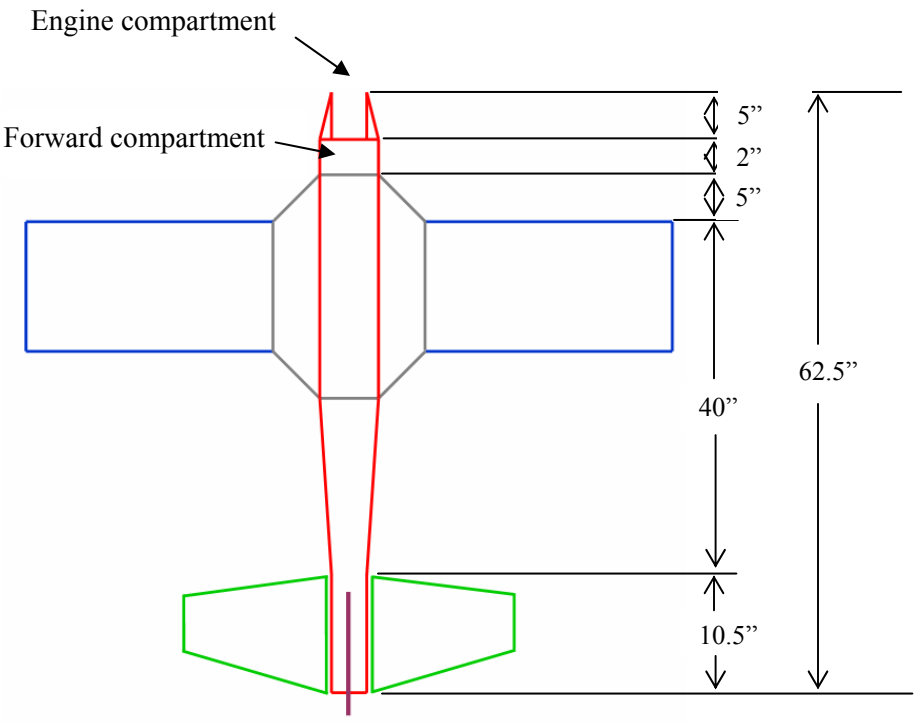


**Figure 2.11** Schematic illustrating the final fuselage dimensions

## 2.9 Control surfaces

### 2.9.1 Ailerons

The initial ailerons size and location were determined by using the guidelines given by Ref.3.3. For the span, the typical value of an aileron extending from 50% to 90% of the wing span was used. This results in an aileron span that is 40% of the half-wing span in the retracted configuration: $b_a = 0.4*33 = 13.2$ inches. The team decided to not implement ailerons on the wing-extensions in order to keep the design simple for construction. However, the aileron span was increased to $b_a = 14$ inches to account for the span-extended configuration. It could not be increased more because of the space required for flaps.

The aileron chord was determined using the following figure from Ref. 2.3:

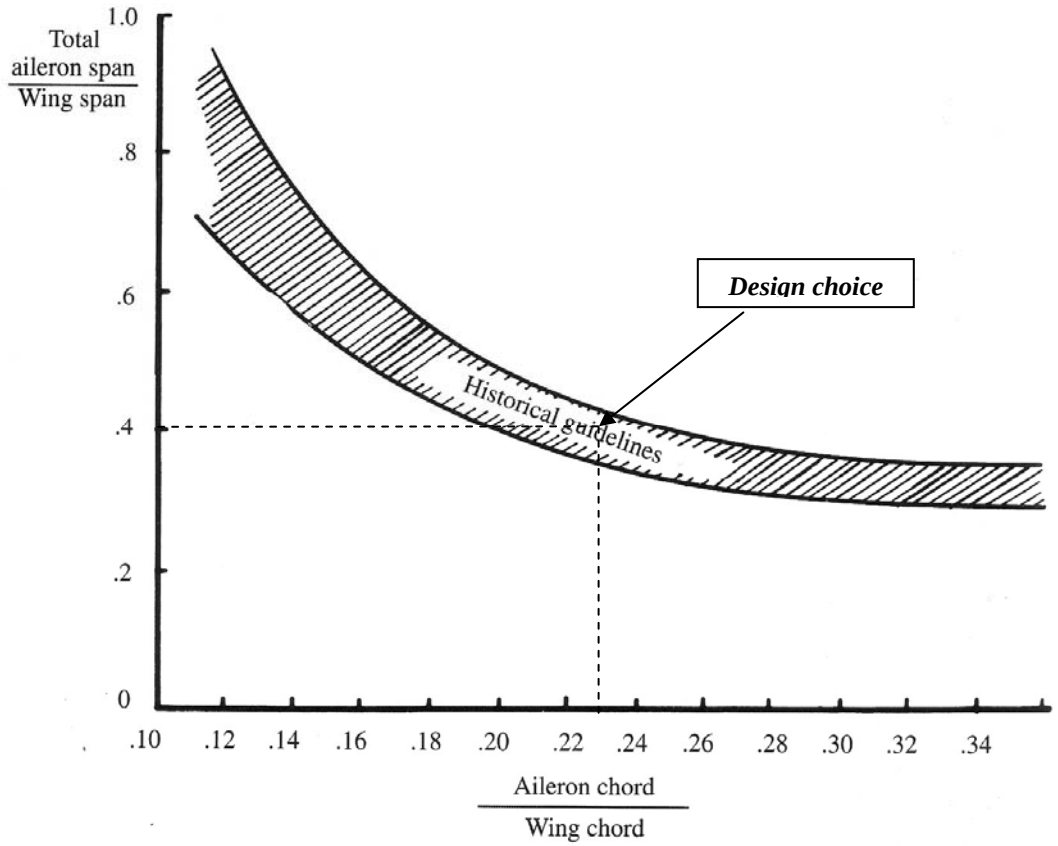


**Figure 2.12** Guidelines used to size the ailerons (from Ref.2.3)

For an aileron span that is 40% of the wing span, the figure shows aileron chord that range from about 20% to 26% of the chord. A value of 23% was chosen, resulting in an aileron chord of: $c_a = 0.23*13 = 2.99$ inches.

### 2.9.2 Elevator

In order to increase the "elevator" effectiveness, an all-moving tail was selected. This choice came from the need to have large control power to trim the aircraft in the wing-swept configuration (dash). As previously discussed, results obtained from numerical simulations (VLMpc) show that the backward shift of the aerodynamic center induced by the sweep of the wings is expected to be greater than the backward shift of the aircraft center of gravity. This will result in a larger moment arm, and thus in a larger moment produced by the wing that the tail will have to counterbalance. Therefore, an all-moving

tail was chosen, providing a variable tail incidence and thus a tremendous “elevator” effectiveness to trim the reward shift of the aerodynamic center.

In addition, the tail moment arm was increased from 33.6 inches (initial sizing) to about 39.4 inches in order to maintain a reasonable value for the wing-swept configuration. As a result, the distance between the aerodynamic center of the wing and the aerodynamic center of the horizontal tail that is about 65% of the fuselage length in loiter configuration, 63% in take-off configuration and about 54% in dash. These values accounts for the movements of the wing aerodynamic center estimated by VLMpc. In the same way as the choice of an all-moving tail, this increase of the tail moment arm compensates the increase of the nose-down moment induce by sweeping the wings and ensures a sufficient tail power to trim the aircraft in all its different flight configurations.

### 2.9.3 Rudder

The initial sizing of the rudder was based on the guidelines given by Ref.2.3, according to which rudders generally begin at the side of the fuselage and extend to between 90% and 100% of the tail span. It was chosen to have the rudder extending all the way to the tip of the tail to facilitate the construction. Rudders being generally about 25-50% of the tail chord, a value of 40% was arbitrarily selected for the VT Morphing aircraft. Finally, the rudder is tapered in chord by the same ratio as the tail surface so that it maintains a constant percent of chord. It must be noticed that this initial sizing was kept as the final sizing for the rudder. Indeed, no specific requirement was given to the team concerning control effectiveness. In addition, due to time constraint, no lateral-directional dynamic analysis of the aircraft was performed. However, the dimensions have been selected near the maximum typical values and are thus conservative.

## 3. Actuation

### 3.1 Span

As stated earlier the main goal was to create a wing of an airplane that can produce three changes in shape. The first aspect of the wing changing that will be

discussed is the span. To implement this change our team last semester decided through much design work to use a wing extension housed inside the main wing to increase the span length. Last semester our five foot wing had inside of it a 12 inch extension that extended out of the wing a maximum of 10 inches. This span extension was actuated by a winch servo that was counter wrapped with fishing line. When the winch servo was rotated, one side of the fishing line would unwrap while the other side wound up. Since this fishing line was attached to opposite ends of the wing extension, a pull-pull method could be used to actuate the span. Figure 3.1 shows last semesters span extension setup.

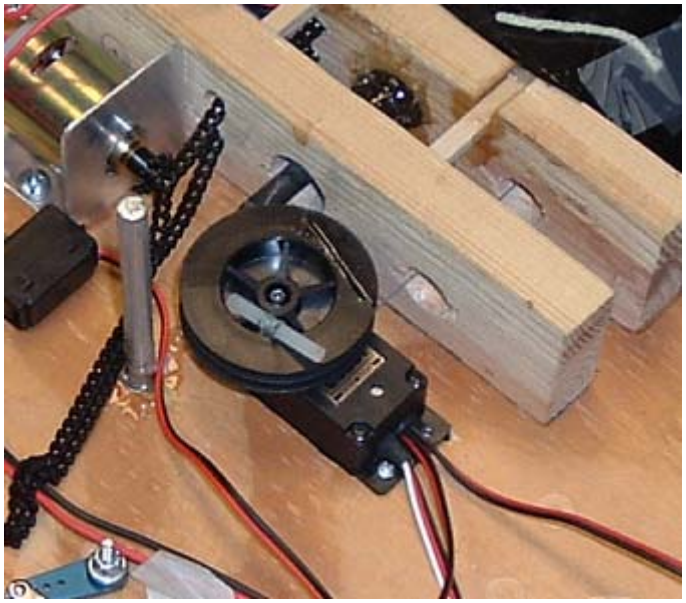

**Figure 3.1.** Span actuation setup from last semester. Notice the counter-wrapped servo head.

This method of using a counter-wrapped servo and a pull-pull method for moving the span extension worked very well. With the simple movement of the control stick on the remote, the span could be extended or retracted with ease every time. When evaluating which method to use this semester for the span extension, our group had an easy time deciding. Due to the simplicity of the design and the small amount of equipment needed for actuation, we once again decided to go with the winch servo setup.

As stated earlier our goal for this semester was to create a model airplane which had wings that could implement three changes. Our group wanted to make the changes much more significant than last semester in order to get a wider range of performance

from them. This goal made us increase the size of the extension so we could get very close to a 50% increase in span size. This is a big difference from the approximately 20% increase from last semester. Using the counter-wrapped servo method for actuation the amount of span extension that is pulled out of the wing is determined by the amount of fishing line the servo can wind up on its control horn. Since the winch servo has only a maximum of three rotations, the determining factor of how much we could extend the span is the circumference of the control horn. Using the equation for the circumference of a circle, we were able to Figure out what diameter the control horn needed to be so we could get the span extension we were shooting for. Our group found that in order to achieve a span extension of 18 inches the control horn needed to be a diameter of three inches.

### 3.2 Span Actuation Construction

Our group was not able to find any stores that sell circular control horns this size, so we had to make it ourselves. To do this our team bought a spool of fishing line that was exactly three inches in diameter. All that needed to be done was unwrap the existing fishing line on the spool and then attach it to our servo head. Figure 3.2 shows a picture of the completed control horn that we manufactured.

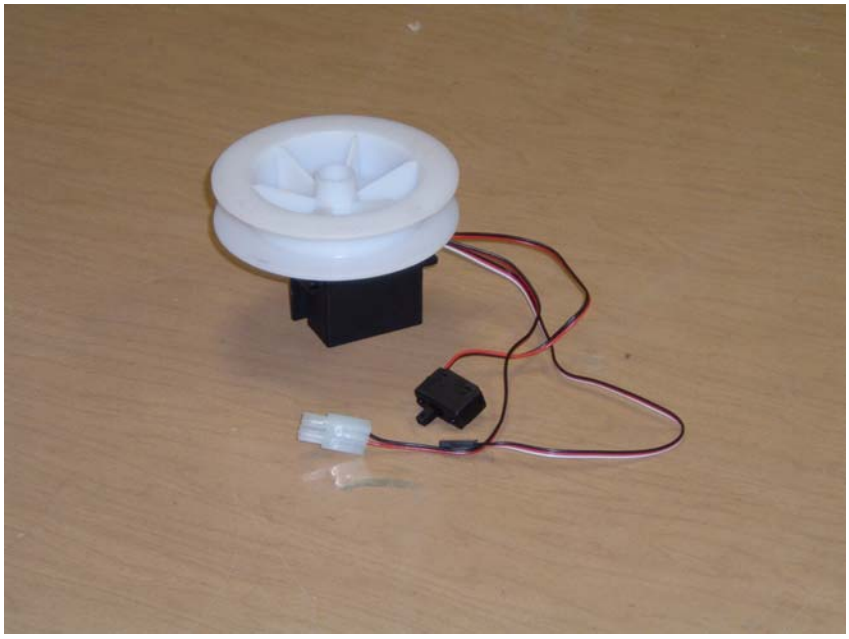

**Figure 3.2.** Completed control horn that was used to actuate the span extension in conjunction with the winch servo.

### 3.3 Chord

Last semester's design included an extension that would increase the length of the chord of the wing. With the use of three chain driven power screws, the trailing edge of the wing extended back approximately 5 inches. This configuration would aid during take off and landing so the wing could produce more lift and fly at slower speeds. During the construction of the wing our group ran into a few problems. The main problem was that we were not able to make the entire trailing edge of the wing expand to increase the chord length. We weren't able to do this because of the span extension in the outboard part of the wing. The ribs in that section would not be able to structurally support both an extension in span and extension in chord length. The ribs became too thin and broke very easily after being cut up to support both shape changes. The solution for this last semester was to only have the inboard section of the wing up to the span extension increase in chord length.

The next problem our team ran into was the actuation of the chord extension. A combination of the motor being undersized and there being too much friction in the power screw setup caused the chord extension not to be able to move. The extension worked great when the chain to drive it was moved by hand, but when the motor was

used, nothing moved. Figure 3.3 shows a picture of the design and setup for chord actuation from last semester.

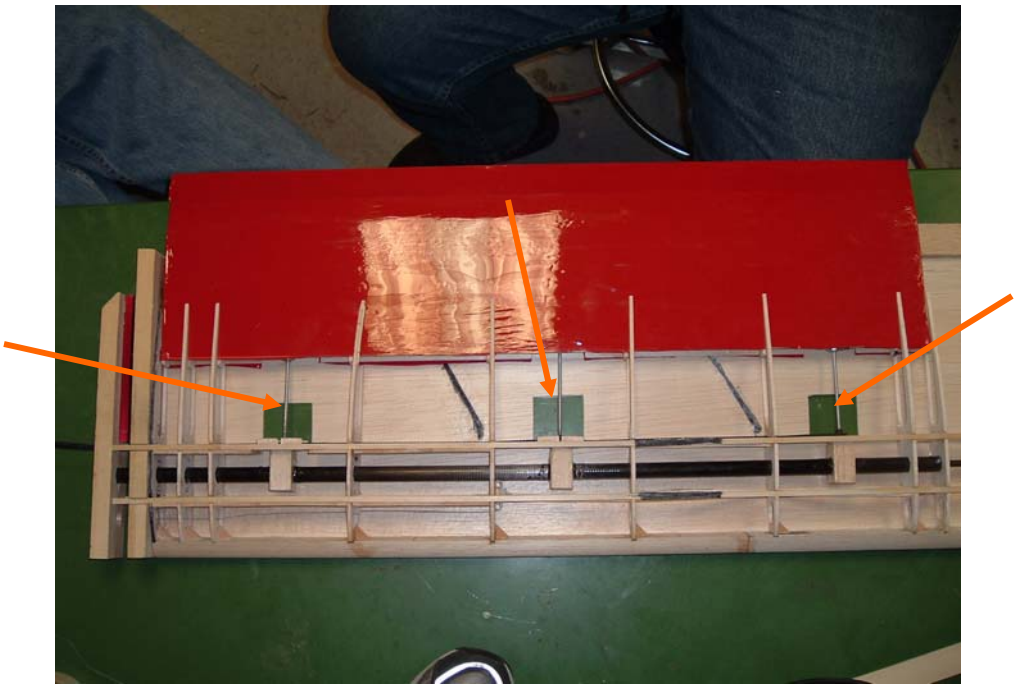

**Figure 3.3.** Chord actuation setup from last semesters design. The arrows point to the three power screws.

This design of extending the chord was also tested in the wind tunnel last semester to see what advantages or disadvantages it would produce. The results showed that extending the chord the distance we did, did not have much of an effect. Based on these wind tunnel tests, and the problems we encountered while building this design, our team decided to go at chord extension with a different approach.

Using a slotted flower flap design the plane would gain more of an increase in performance than with a chord extension like we originally designed. A slotted fowler flap design would also be easier to implement and actuate on our wing. These two facts were enough for our group to decide to use this as our chord extension. Since a fowler flap is the trailing edge of the wing extending out and downward, we were able to still consider this an increase in chord size. Figure 3.4 shows a picture of what a slotted fowler flap looks like.

**Figure 3.4.** Slotted fowler flap. The trailing edge extends out and downward increasing the chord length.

Most modern day airplanes use a four bar linkage to implement fowler flap systems. Since we are constrained with the amount of space inside of the wing and also weight, we decided to use a type of sliding track that the flap will follow. Thin metal rods were curved in the shape we wanted the flaps to follow and were attached to the main wing. The flaps have tracks inside of them that when actuated, will follow along the curved metal rod's path. This will extend the flap out and downward at the same time.

The actuation of the flap was a lot easier than the actual construction of it. The only real movement that was needed was the push or pull of the flap along the pathway of the metal rod. This movement was created by a small servo with a control horn on the top. The movement of the servo was transferred through a flexible control rod. The flexible control rod is a flexible metal wire that is inside of a plastic tube. The wire is able to be bent around corners but is still able to transfer movement from a servo to the flap system. We were able to house the servo almost anywhere we wanted while still being able to actuate the flaps.

### 3.4 Sweep

The sweep actuation design is derived directly from the full size wind tunnel model used in the team's previous testing. The sweep mechanism centers around an axially constrained power screw which drives a transverse nut up and down its length. The sweep block, as shown in Figure 3.5 is rigidly connected to the transverse nut. The sweep block itself stays level and produces the desired linear motion needed to sweep the wings. A fully dimensioned CAD drawing is shown in Figure A-1 in Appendix A.

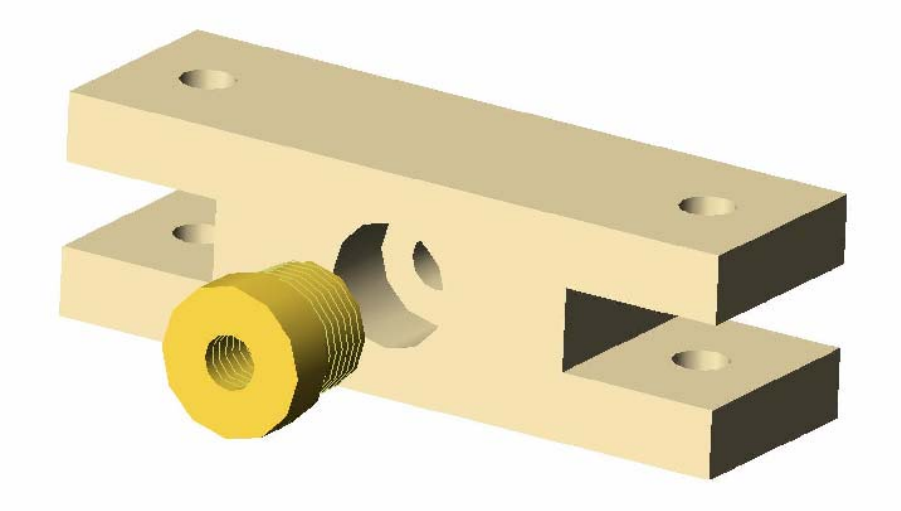

**Figure 3.5** AutoCAD drawing of sweep block. The power screw is threaded through the sweep nut, shown here in yellow.

The sweep block is connected to the wing structure with two ¼" carbon fiber rods. The rods are connected to the wing and the sweep block with plastic ball joints and nylon bolts. Since the ball joints act as revolute joints, the sweep rods can be considered two force members during this analysis. As the sweep block moves forward, towards the nose of the plane, the rods rotate and move towards the center of the fuselage, causing the wings to sweep back. Figure 3.6is an AutoCAD drawing of the power screw and sweep block.

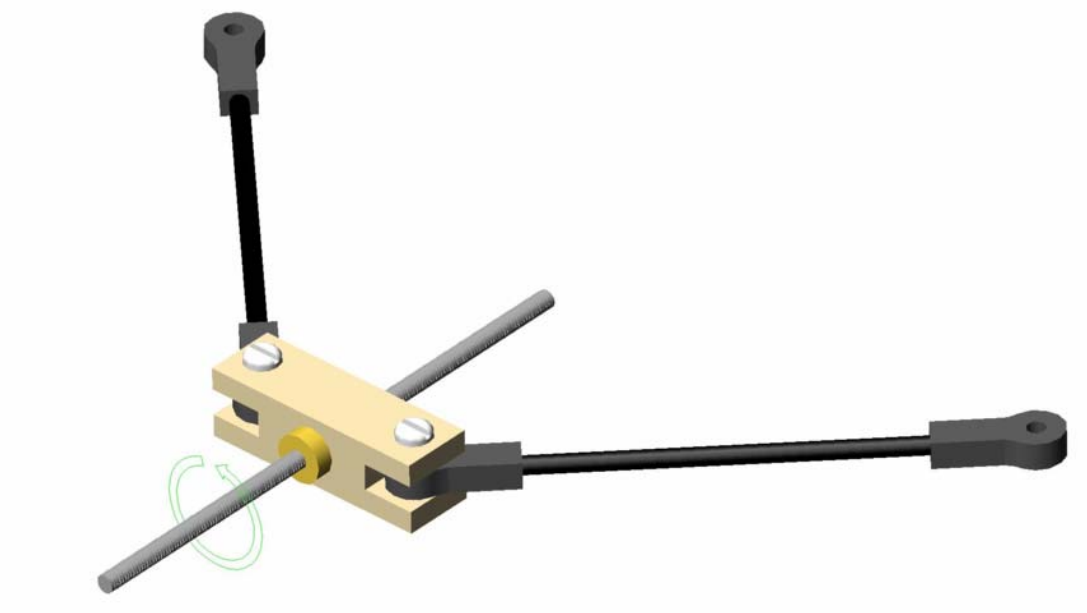

**Figure 3.6** AutoCAD drawing of sweep mechanism. The power screw rotates while the sweep block moves axially.

The power screw is driven by a DC electric motor. To calculate the motor specifications the load applied to the power screw needed to be found. The maximum load transmitted to the sweep block will occur when the aerodynamic drag is at a maximum. Once the load is known the torque required to raise the power screw (sweep the wings forward) is given by the equation:

$$T_{raise} = \frac{Fd_m}{2}\left(\frac{l + \pi f d_m}{\pi d_m - fl}\right) \tag{3.1}$$

where $T_{raise}$ is the torque required to lift the load, $F$ is the load transmitted to the sweep block, $l$ is the lead of the power screw, $f$ is the friction factor between the nut and the power screw and $d_m$ is the mean diameter of the power screw. This torque represents the minimum torque requirement for the DC motor.

The torque required to lower the power screw (sweep the wings backward) is given by the equation:

$$T_{lower} = \frac{Fd_m}{2}\left(\frac{\pi f d_m - l}{\pi d_m + fl}\right) \tag{3.2}$$

where $T_{lower}$ is the torque required to lower the load, $F$ is the load transmitted to the sweep block, $l$ is the lead of the power screw, $f$ is the friction factor between the nut

and the power screw and $d_m$ is the mean diameter of the power screw. The power screw efficiency is given by the equation:

$$e = \frac{Fl}{2\pi T_{raise}} \tag{3.3}$$

where $e$ is the mechanical efficiency, $T_{raise}$ is the torque required to raise the load, $F$ is the load transmitted to the sweep block and $l$ is the lead of the power screw.

The final factor of interest is determining wither or not the power screw is self-locking, or non-back-drivable. The self locking condition is of the form:

$$\pi f d_m > l \tag{3.4}$$

where $f$ is the friction factor between the nut and the power screw, $d_m$ is the mean diameter of the power screw and $l$ is the lead of the power screw. As long as this condition holds there is no need for a holding torque to be maintained by the motor during non-transitional flight. Table 3.1 shows the results of the power screw calculations.

**Table 3.1:** Calculation results for sweep power screw.

| Power Screw Calculations | |
|---|---|
| Screw Specifications | |
| Axial Load (lb) | 20 |
| Mean Diameter (in) | 0.25 |
| Lead (in) | 0.0625 |
| Friction Factor | 0.1 |
| Screw Material | Stainless Steel |

| Torque Results | |
|---|---|
| Total Torque to Raise (ft-lb) | 0.037712076 |
| Total Torque to Lower (ft-lb) | 0.004221103 |
| Efficiency (%) | 43.96109015 |
| Self Locking | YES |
| | |
| Total Torque to Raise (N-mm) | 51.13071005 |
| Total Torque to Lower (N-mm) | 5.723047151 |
| Total Torque to Raise (in-lb) | 0.452544917 |
| Total Torque to Lower (in-lb) | 0.050653235 |

The results from table 3.1 can now be used to determine the motor specifications. The motor must be able to sustain a torque in excess of 0.45 in-lbs, or 51.1 N-mm, to sweep the wings forward. The torque to lower the load, sweep the wings back, is only a fraction of that required to sweep forward because the drag forces are actually helping to sweep the wings. The power screw is also self locking; since no holding torque is required the motor does not have to be active when the wings are not morphing. This will result in increased battery and motor life.

Finally, the motor must be able to exert the required torque at a high enough RPM to actuate the wings in an acceptable amount of time. The time required to sweep the wings forward, the worst case scenario, is given by the equation:

$$t_{sweeo} = \frac{\Delta x_{sweepblock}}{l\omega} \tag{3.5}$$

where $t_{sweep}$ is the time required to sweep the wing, $\Delta x_{sweepblock}$ is the distance the sweep block translates, $l$ is the lead of the power screw and $\omega$ is the rotational speed of the motor at the torque required to sweep the wing. From this equation, if the motor rotates at 1200 RPM the time required to sweep the wings forward is approximately 5.6s.

### 3.5 Wing Box

The sweep actuation demands a sturdy support structure for the wing and fuselage connecting points. The core of the aircraft, which we termed the wing box, is a rigid structure that connects the wings, the fuselage and all the mechanical actuation together. The wing box is formed from two sheets of 1/8" plywood that have been covered with layers of carbon fiber. To reduce the weight of the wing box excess material was cut away. Figure 3.7is a drawing of the wing box with the sweep block positioned inside. A fully dimensioned AutoCAD drawing is shown in Figure A-2 in Appendix A. The wings, not shown, pivot around rods that pass through the wing box. The two carbon fiber pieces are separated by plastic spacers and held together with nylon bolts. For added strength a ¼" carbon fiber rod was placed across the pivot points.

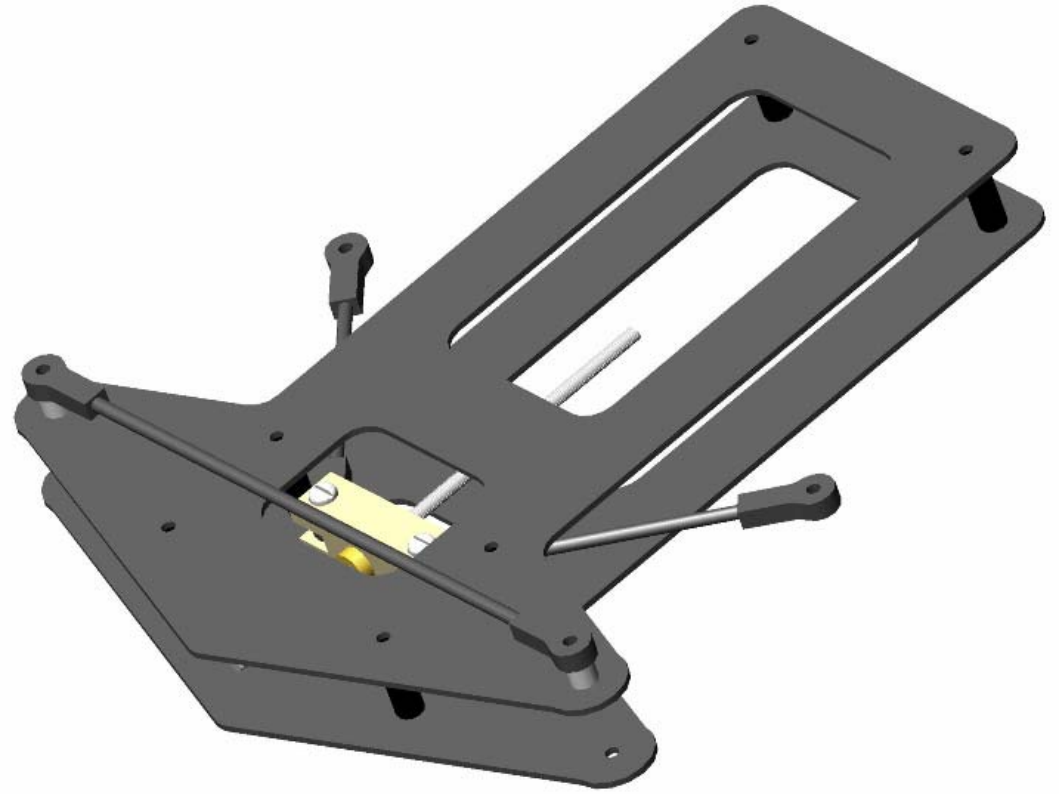

**Figure 3.7** AutoCAD drawing of wing box and sweep block. The nylon screws that connect the two carbon fiber pieces are not shown.

The lengths of the connecting rods are determined by the location of the sweep block and the available actuation space within the wing box. In order to avoid the plastic spacers and still reach the maximum sweep angle of 45 degrees, the connecting rods needed to be approximately 6 ½" long from pivot to pivot.

To mount the motor and power screw within the wing box, prefabricated sheet metal brackets were used. One bracket is positioned in the tail section of the wing box and houses a ¼" ball bearing. This bracket simply keeps the power screw directly in the center of the wing box. A second bracket is attached to the front of the box and serves as a motor mount. Figure 3.8 is an AutoCAD drawing that shows the motor mounted to the wing box. The motor shaft is connected directly to the power screw with a ¼" Hooke's coupling. This coupling allows for slight misalignments in the drive system. A fully dimensioned CAD drawing is shown in Figure A-3 in Appendix A. Figure 3.9 is an image of the sweep actuation, with the wings, at zero and 45 degrees of sweep.

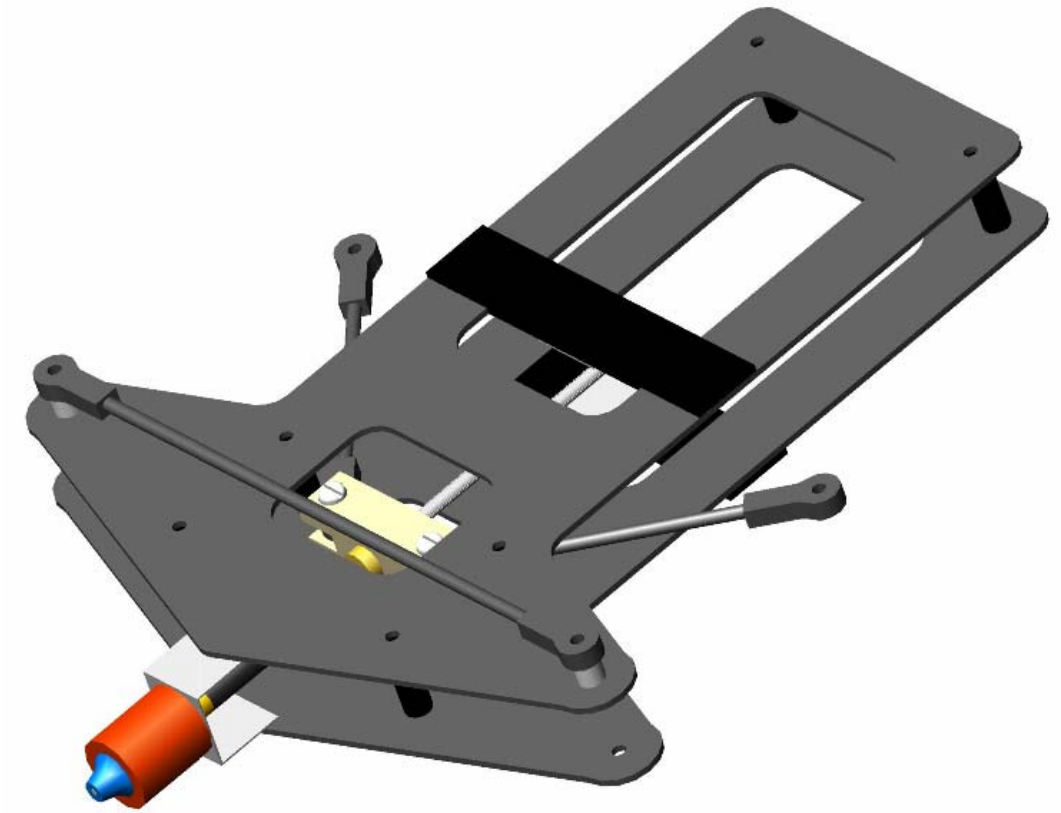

**Figure 3.8.** AutoCAD drawing of wing box with motor. The electronic speed control and kill switches are not shown and will be discussed in detail later.

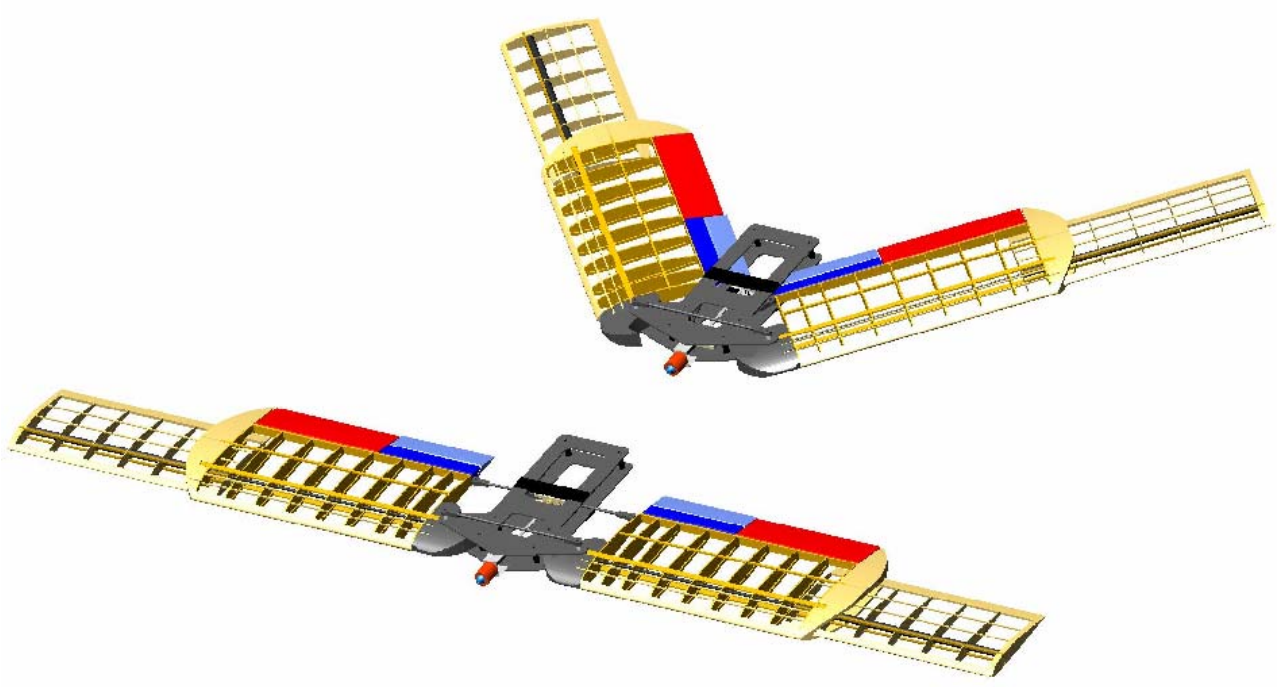

**Figure 3.9.** AutoCAD drawing of wing box with wings. Sweep angles of 0 and 45 degrees are shown.

### 3.6 Sweep Construction

The first step in the fabrication of the sweep mechanism was to cut the sweep block from a piece of bass wood. The construction was directly in accordance with Figure A-1 in Appendix A. After the block was cut we permanently attached the sweep nut to the sweep block using 30 minute epoxy. Figure 3.10 is an image of the sweep block after construction.

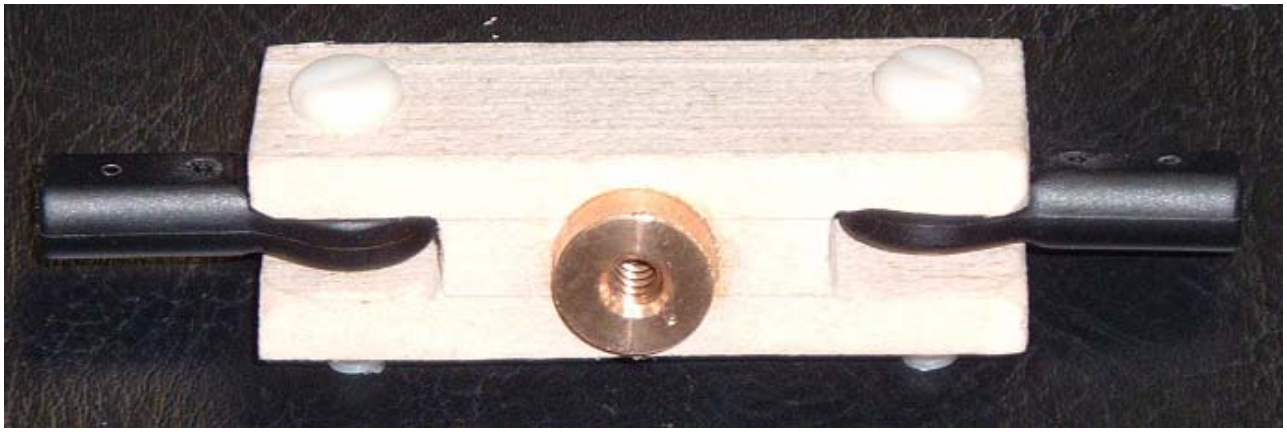

**Figure 3.10.** Image of sweep block. The bronze sweep nut was connected to the block using 30 minute epoxy.

To build the carbon fiber plates the team first cut out the shape shown in Figure A-2 of Appendix A from 1/8" plywood. The team then took a sheet of carbon fiber and coated it and the plate with resin. To maximize the effectiveness of the carbon fiber we positioned the crosshatching at an angle of 45 degrees as shown in Figure 3.11. By applying the carbon fiber at an angle we not only increased the tensile and compressive strength but also its strength in bending. For extra strength a second coat was applied to the upper portion of the top plate. Once the resin was totally dry, all the excess material was removed to reduce weight.

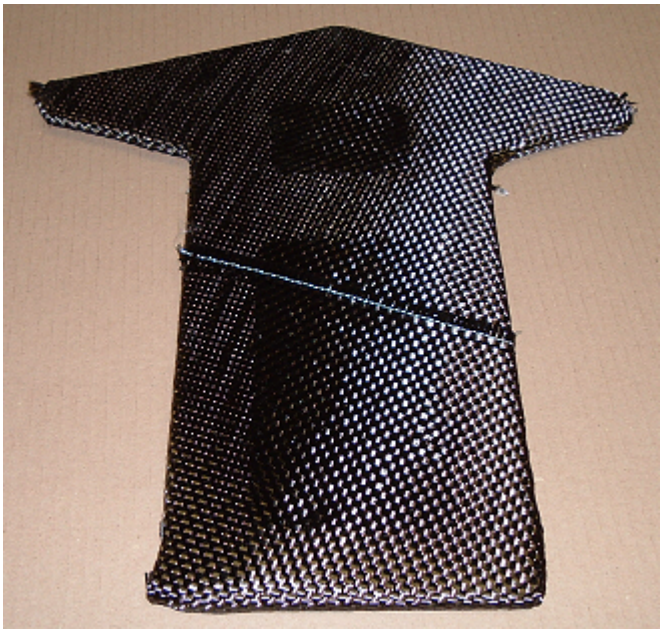

**Figure 3.11.** Image of sweep box plate covered with carbon fiber. The carbon fiber was applied at a 45 degree angle to increase its strength.

The first step in fabricating the carbon fiber push rods was to bore out the threads of the ¼" ball joints. Then the ¼" solid carbon fiber rods were cut to length and glued into the ball joints. The sweep push rods were cut to total lengths of 6 ½" while the wing box reinforcement bar was cut to a total length of 13 1/3".

To attach the wings to the pivots on the wing box, 1 ½" thick blocks were cut out of bass wood. To keep the leading edge of the root wing from stalling we cut an arc that would form a circle as it was exposed to the air flow during flight. The blocks were then fitted with low friction ball bearings at the top and bottom contact surfaces. Figure 3.12 is an image of the wing mounting blocks after construction.

**Figure 3.12.** Image of wing mounting blocks. The arced edge maintains a smooth profile as the wing is swept back.

The plastic spacers to separate the wing box were cut from ½" diameter, 1/16" thick, PVC piping. The motor mount and power screw mount were each made from prefabricated pieces of sheet metal. Increasing the diameter of existing holes was all that was necessary. The final step in the sweep construction was to assemble the individual parts in accordance with Figure A-3 of Appendix A. Figure 3.13 is an image of the sweep mechanism upon completion.

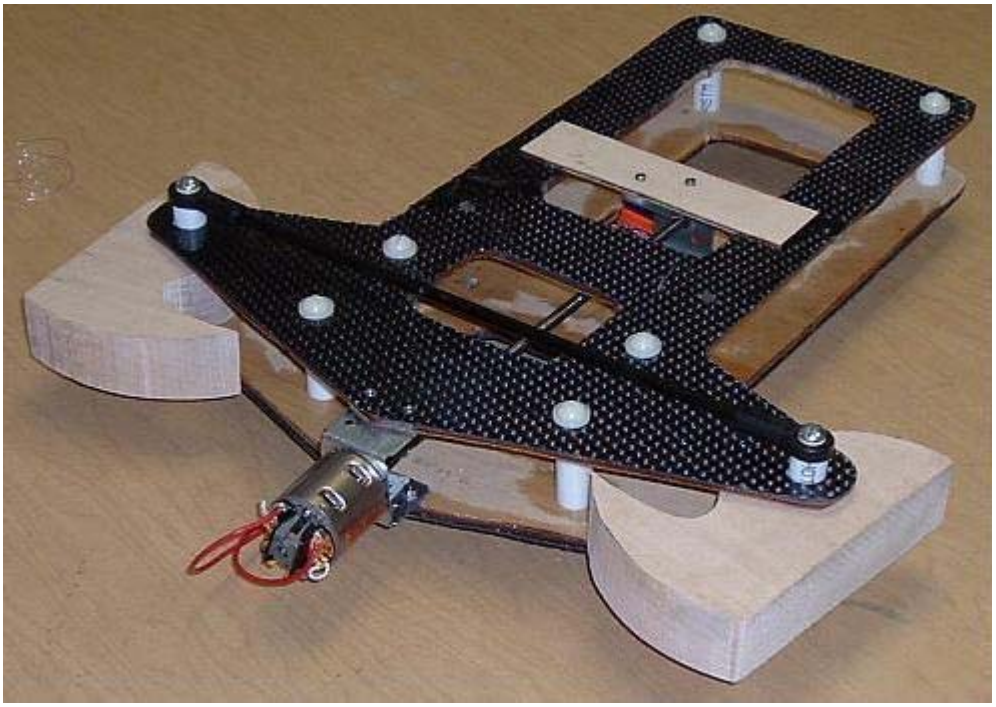

**Figure 3.13.** Image of sweep mechanism after construction. The wings, not shown, attach to the basswood blocks.

### 3.7 Sweep Actuation Electrical System

As stated earlier, last semester our team had a problem with the actuation of the sweep. This was mainly caused by an underpowered motor used in the actuation. This semester our team used a bigger motor with more torque. In order to control the speed of this motor, an electronic speed controller was needed instead of just a small potentiometer. This was due to the current associated with the battery pack for the motor. Figure 3.14 shows a diagram of the electrical system and how it was setup. As you can see from the diagram, the current starts off at the battery and flows to the speed controller. Here the current is regulated to determine the speed of the motor. Next it travels to the first kill switch. The kill switch is placed near the beginning or end of the power screw to stop the motor; which stops the sweeping of the wing. When compressed the kill switch will stop the flow of current to the motor. When the speed controller reverses the polarity of the current, the motor is allowed to spin in the opposite direction. This is due to the Zener diode that is connected to the kill switch. Zener diodes act as check valves that allow current to flow in only one direction through them. When the circuit is broken due to the kill switch being tripped, the Zener diode is now placed into

the circuit. Since the speed controller reverses the flow of current through the system, the motor is allowed to turn due to the Zener diode. The motor pulls the sweep block away from the kill switch until it is disengaged which allows current to flow through the original circuit.

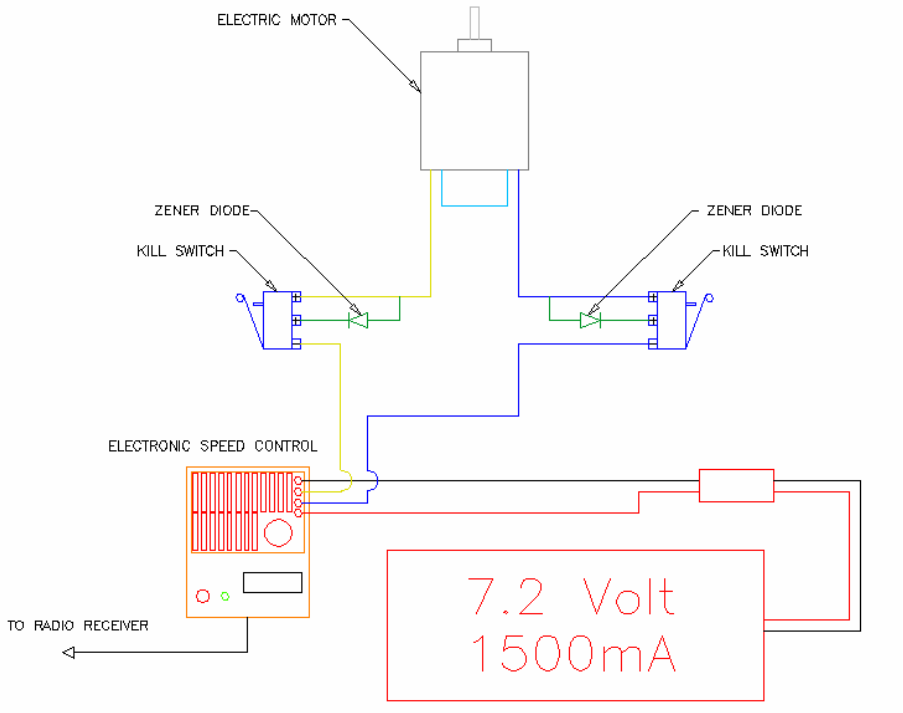


**Figure 3.14.** Sweep actuation electrical system. Notice the Zener diodes in the circuit that act as check valves and allow current flow in only one direction when engaged.

# 4. Structures

## 4.1 Wings

The main purpose of the wings of the aircraft is to create the lift that will enable it to fly. The airfoil shape of the wing is created by a number of ribs spaced evenly throughout the wing. These ribs are then covered by monokote to create a smooth airfoil shape. The ribs were cut out of 1/8$^{th}$ in. thick balsa wood. These ribs were glued to a leading and trailing edge stock to complete the airfoil shape. To add support to the wing so it is able to transfer aerodynamic loads to the fuselage ¾ inch hardwood planks were used as spars. These planks were glued to the top and bottom of each rib and then are

connected to the turntables. To also increase the strength of the wing, carbon fiber was glued to the top and bottom of these planks. This will increase the bending strength of each wing.

To support the aerodynamic loads created by the wing extension a carbon fiber rod was used. This rod was attached to the turntable and extended along the path the extension would travel. When actuated the extension would slide out of the wing along this carbon rod.

### 4.2 Fuselage

The main mission of most modern aircraft is to carry some type of cargo. The wings and engines are designed to provide the required lift and thrust to transport that cargo in the fuselage. The morphing wing aircraft, however, was designed to demonstrate the ability to morph in flight and the fuselage therefore was designed to support the wing structure, completely reverse from the traditional aircraft.

The fuselage on the morphing wing aircraft, shown in Figure 4.1, was designed to: support the main structural box of the wing, to transfer the loads from the tail to the main structural wing box, to carry the landing loads, and to carry the engine.

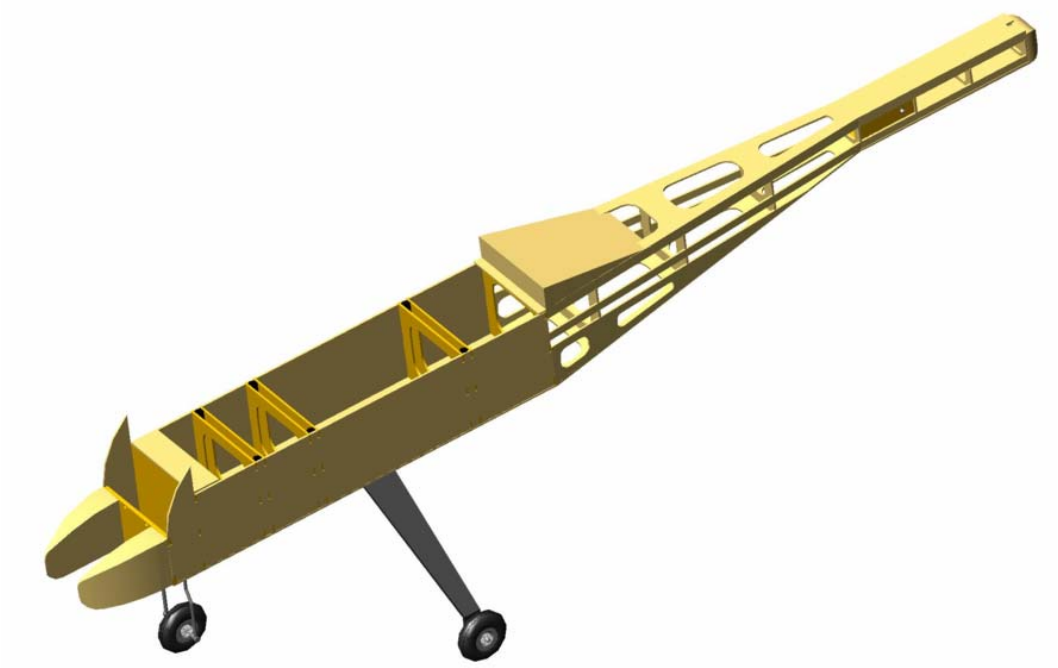

**Figure 4.1**. Full Auto CAD drawing of the fuselage design

### 4.2.1 Wing Box Support

The wing box is supported by a series of three bulkhead pairs, which attach to six; three-inch nylon bolts from the wing box. The bulkheads were constructed from 6” x 5” x 1/8“ ply wood and a 3“x 4“ interior cut out was made in each bulkhead to save weight. The nylon bolts screw into a series of nylon nuts were epoxyed between two bulkheads, shown in Figure 4.2.

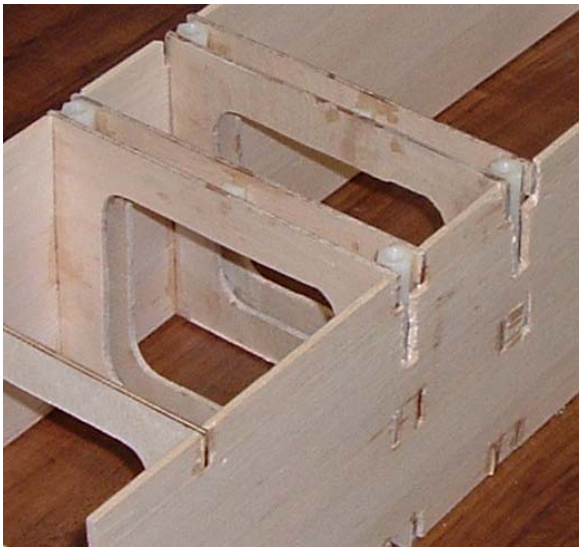

**Figure 4.2**. Photograph of the Structural bulkheads that support the wing box.

Each bulkhead weighed an average of 0.8 ounces and the nylon bolts each weighed an average of 0.02 ounces. The first set of bulkheads used a series of six nylon nuts, the middle bulkheads used seven nuts and the far aft bulkheads used four nuts. The greatest number of nuts were used at the midsection, as this is where the greatest loads from the wing box would occur. Four bolts were used in the aft section because it sustains the lowest loads and this is the exact number required to fully cover the bolts. Six and seven nuts were used in the forward section to provide greater structural integrity between the bulkheads where the loads were the greatest.

Five other nuts were used as spacers at the other corners and at the midsection of each bulkhead to provide structural integrity. These bulkheads were then attached to the baseboard, which was made of 1/8“ plywood; and was also attached to the sides which was made of 1/8“ balsa.

### 4.2.2 Tail loads

The trim and directional control loads from the tail are transferred to the body by a series of balsa bulkheads, four stiffening rods, and the top and bottom sheets as shown in Figure 4.3.

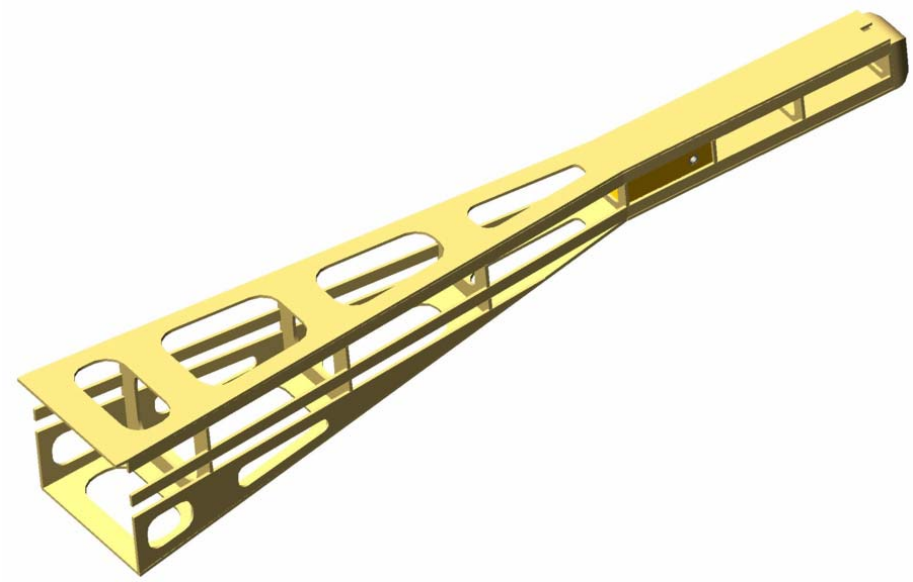

**Figure 4.3**. AutoCAD Design of the aft fuselage.

Three balsa bulkheads decreasing in size, forward to aft, support the aft portion of the fuselage. Four stiffening rods positioned in each corner and running the length of the aft fuselage attach these bulkheads to one another. These same stiffening rods attach the aft fuselage to the forward bulkheads.

### 4.2.3 Landing Loads

The landing loads are carried between the landing gear and the gear's structural support. The main landing gear is made from ESD carbon fiber, which provides high strength and the flexibility to absorb hard landings, while only weighing 3.15 ounces. The landing gear corners are also reinforced to provide improved shock control, as shown in Figure 4.4.

**Figure 4.4**. Photograph of the reinforced landing gear corners

The landing gear is attached to the fuselage by four-¼“ bolts attached to a ¼“ sheet of plywood. The plywood support is then attached to the structural bulkheads, which carry the load through to the main structural box.

The forward landing gear is attached to the second most forward bulkhead as well as through the 1/8“ plywood base plate. The forward gear is attached to a servo and is used to steer the plane while it is moving on the ground.

### 4.2.4 Engine Loads

The engine is mounted to the forward most ¼“ bulkhead, shown in Figure 4.2, with four bolts that carry the engine mounting harness. The ¼“ bulkhead is then attached to the 1/8“ plywood base plate as well as to the 1/8“ balsa siding. The bulkhead, as well as the siding, was covered with epoxy hardener to prevent leaking fuel from seeping into the wood.

The fuel tank for the engine is set at the CG and is carried within the structural bulkheads. The fuel tank is positioned between the two most forward structural bulkheads and held in place by 1“x 6”x1/8“ balsa sheets above, below, forward and aft of the tank. The fuel lines from the tank pass through a ¼“ radius hole drilled through the forward engine bulkhead.

## 4.3 Wing Box Structural Calculations and Loading Test

VLMpc provides an estimate of the span loading of the wing. Using the following formula we may deduce the span-wise distance of the center of pressure:

$$y_{CP} = \frac{1}{CL_{wing}} \cdot \int_{y_{pivot}}^{b/2} y \times CL(y) dy \qquad (4.1)$$

Since we have a list of values for *Cl(y),* we need to do a numerical approximation of Equation 4.1. The following equation was used:

$$y_{CP} = \frac{1}{CL_{wing}} \sum_{i=1}^{M-1} \frac{(y_i + y_{i+1})(Cl_i + Cl_{i+1})}{2 \times b} (y_i - y_{i+1}) \tag{4.2}$$

Where:

- $CL_{wing}$ is the portion of lift that is produced from the pivot to the tip. This factor is used to correct for the part of the lift that is produced by the fuselage and the wing section inboard the pivot. $CL_{wing}$ is defined by Equation 4.3.3.

$$CL_{wing} = \frac{\int_{y_{pivot}}^{b/2} Cl(y)dy}{b/2 - y_{pivot}} \tag{4.3}$$

- The subscript *i* corresponds to the i[th] rank in the table of the span loading provided by VLMpc.

The results of the VLMpc calculations are provided in table 4.1. This table gives the value of the local lift coefficient *Cl(y)* (or *CL(y) /CL*. *b*/2) at the given span-wise distance *y*.

**Table 4.1:** Y-Y Pivot vs. Cl for three different wing configurations

| Loiter | | Maneuver | | Dash | |
|---|---|---|---|---|---|
| Y-Y Pivot | Cl | Y-Y Pivot | Cl | Y-Y Pivot | Cl |
| 43.5 | 0 | 25 | 0 | 26.87 | 0 |
| 41.543 | 0.436 | 23.746 | 0.426 | 25.54494 | 0.121 |
| 37.5775 | 0.591 | 21.205 | 0.606 | 21.68727 | 0.362 |
| 33.612 | 0.68 | 18.664 | 0.721 | 15.98732 | 0.604 |
| 29.6465 | 0.745 | 16.123 | 0.803 | 9.534728 | 0.845 |
| 26.3505 | 0.8 | 13.582 | 0.866 | 3.695663 | 1.044 |
| 23.003 | 0.923 | 11.041 | 0.915 | 0 | 1.138962 |
| 19.0375 | 0.983 | 8.401 | 0.956 | | |
| 15.072 | 1.025 | 5.728 | 0.991 | | |
| 11.158 | 1.059 | 3.187 | 1.021 | | |
| 8.068 | 1.083 | 0.976 | 1.048 | | |
| 5.0295 | 1.108 | 0 | 1.064093 | | |
| 1.5275 | 1.14 | | | | |
| 0 | 1.237184 | | | | |

The goal of the loading tests is to demonstrate the ability of the structure to withstand a load factor of:

- at least 4 G's in maneuvering
- at least 2.5 G's in loiter
- 2 G's in dash.

For each test, we want to represent the loads that will occur in flight. In order to reproduce the flight conditions the team has use the following test bed:

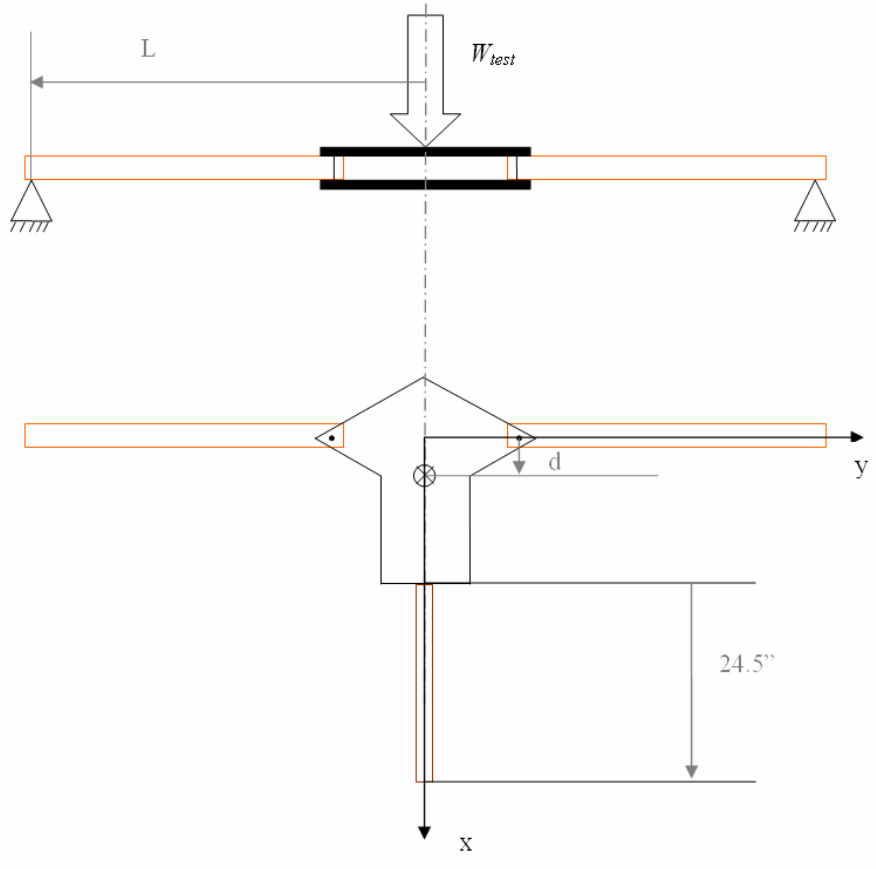


**Figure 4.5:** Description of structural test bed.

The weight has to be placed at an x position of d = 4.3" (aft of the pivot point). The weight to be applied has to be varied as a function of the load factor to be tested. Using VLMpc data in equation 4.1 and 4.2 we obtain the following values in Table 4.2:

**Table 4.2:** Cl percentage vs. Length 'L' from picture above. L is the y-distance between the pivot point and the center of pressure.

| Configuration | CL% | Length (in.) |
|---|---|---|
| Maneuver | 82.12% | 8.2 |
| Loiter | 86.13% | 18.4 |
| Dash | 66.95% | 7.7 |

The weight distribution in the aircraft is the following:

- 4lb in the sweeping wings (subscript w).
- 11lb in the rest of the aircraft (will be referred as fuselage or subscript f).

By definition the load factor is defined as:

$$L = n \times W_{tot} \tag{4.4}$$

$$L = L_w + L_f \text{ and } W = W_w + W_f \tag{4.5}$$

Since $L_w = CL\% \times L$ then $L_w = L / CL\%$

Using equation 4.3.4 and 4.3.5:

$$L_w = n * CL\% * W_f + n * CL\% x W_w \tag{4.6}$$

The first term, in the right hand side of equation 4.3.6, is the load that is caused by the fuselage. The second term represents loads that are internal to the wing. In a maneuver these internal wing loads are not transmitted by the pivot to the rest of the fuselage. Then the mass that is applied on the structure should only represent the load transmitted on the pivot.

$$W_{test} = \sigma \times n_{\max} \times CL\% \times 11 \text{ . lb} \tag{4.7}$$

$n_{\max}$ is the maximum load factor that wants to be tested. $\sigma$ is the safety factor. In this experiment we want to use a safety factor of 1.5.

**Table 4.3:** Test Schedule

| Configuration | CL% | n | $W_{test}$ (lb) | L (in.) | Observation |
|---|---|---|---|---|---|
| Maneuver | 82.12% | 4.0 | 54.2 | 8.2 | Critical shear force at the pivot |
| Loiter | 86.13% | 3.0 | 42.6 | 18.4 | Critical lateral bending moment at pivot |
| Dash | 66.95% | 2.5 | 27.6 | 7.7 | Critical longitudinal bending moment at pivot |

### 4.3.2 Proposed Wing Box Testing Procedure:

1. Fabricate a rod that is long enough to represent the tail. The point of application of the tail force is 24.5" aft the structure (see Figure 4.1 above).
2. Before putting the weights on the structure, measure the weight of the structure (with the "tail rod"). Try to determine where to put the extra weight to have the CG at 4.3" aft the line between the pivot points
3. Put the supports 32.4" apart. Note: 8.2"+16"+8.2"=32.4"
4. IMPORTANT POINT: Even in the Maneuver and loiter configuration, place the prototype wing at a certain angle of sweep. The reason why this angle is needed is to represent the natural pitching moment of the wing. To find this angle use the following procedure:
    a. Place the structure with the wing and the loads (at the balanced CG position) at the test position between the supports, with the wings in the un-swept position.
    b. In the un-swept position the person at the tail will have to apply a force upward to stabilize the system. Sweep the wings until the person at the tail will have to apply a force downward.
    c. This procedure can not be applied in the swept configuration. For test 3 the prototype wing should just be set at $45^{o}$.

### 4.3.3 Wing Box Testing Results and Discussion

Figure 4.6 shows a picture of the structure during the tests. The procedure described above was closely followed to reproduce actual flight conditions of the structure. The effects of the tests in different configurations were similar. The structure survived the tests without any sign of structural failure or permanent damage. No cracking noise was heard and after visual inspection no sign of crack formation was found on the structure surface.

**Figure 4.6:** Testing of the structure

Only limited deflection of the wing was observed even in test 2 which was supposed to be the most constraining test for this characteristic. The rigidity resulting from the carbon fiber and the carbon rod was found to be satisfactory. Figure 4.7 is an image showing this deflection.

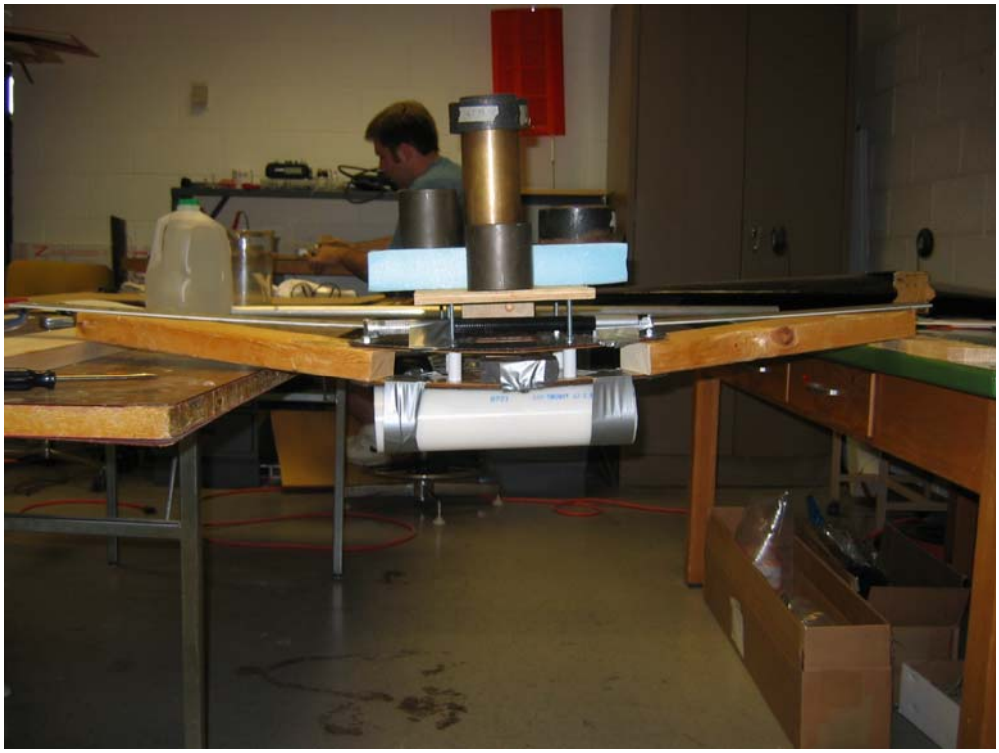

**Figure 4.7:** Deflection due to structure flexibility. During maximum loading now damage was sustained.

The resistance in torsion of the structure was weak. The torque, induced by both the natural pitching moment of the wing ($CM_0$) and the wing sweep, induces a twist of the wing at the pivot level. The maximum twist observed during these tests was about $5^o$. This induced twist will decrease the relative angle of attack of the wing with respect to the fuselage. The consequence of this twist will be an increase in the fuselage drag during the maneuver configuration due to artificially increasing its angle of attack. Figure 4.8 is an image taken from the side during testing that shows the maximum twist deflection.

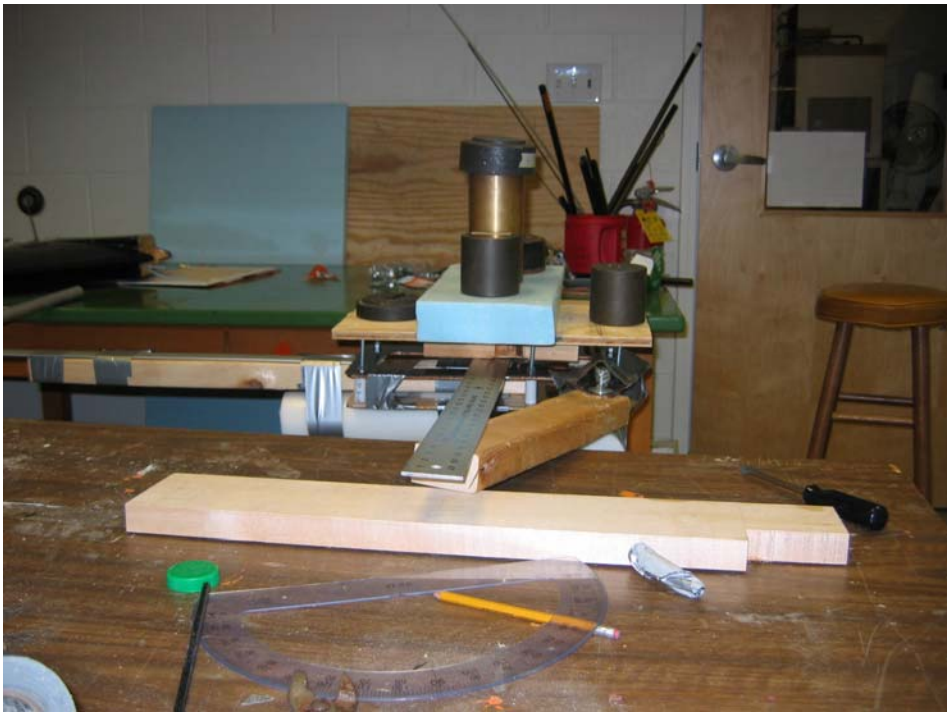

**Figure 4.8:** Side view of the structure under testing. This was the maximum twisting deflection.

### 4.3.4 Wing Box Test Conclusion

This test has shown the ability of the wing box structure to withstand load factors between 0 and 4 G's in the maneuver configuration, 0 and 3 G's for the loiter configuration and 0 and 2 G's in the dash configuration.

The structure was shown to be resistant in bending but relatively weak in torsion. Some discrepancy in performance is expected due to the flexibility in twist but the overall structural characteristics will enable safe flight capability as long as the load factor remains within the flight envelope stated above.

There are some limitations to the conclusions drawn for this test. All the elements in the structure were not the same as those that will be used in the final version of the structure. These differences are:

- A hollow carbon fiber tube was used in the test instead of a thinner but full rod of carbon fiber.
- The material used in the four aft bolts used to connect the structure plates was steal for the test and will be made of nylon in the final design.

The consequence of the change of the carbon rod should not induce significant changes in structure characteristics. But the nylon bolts might decrease the resistance of the structure in bending.

# 5. Aerodynamics

### 5.1 Xfoil Analysis

Analysis of the chosen Clark Y airfoil was conducted using Xfoil. The properties determined by this analysis are the maximum lift coefficient, the zero lift angle of attack, the lift curve slope and the drag polar. The input required to run this analysis are the coordinates of the Clark y airfoil, the Reynolds number, and the Mach number. However, since the speed range at which the aircraft will operate has not been determined a range of speeds was used to calculate the Reynolds number and the Mach number. Table 5.1 lists the speed ranges and the corresponding Reynolds and Mach numbers.

**Table 5.1:** Speed ranges used of the analysis

| Velocity (mph) | Velocity (ft/s) | Reynolds number | Mach number |
|---|---|---|---|
| 30 | 44.0 | 268065 | 0.0397 |
| 40 | 58.7 | 357420 | 0.0529 |
| 50 | 73.3 | 446775 | 0.0661 |
| 60 | 88.0 | 536130 | 0.0794 |
| 70 | 102.7 | 625486 | 0.0926 |
| 80 | 117.3 | 714841 | 0.1058 |
| 151.2 | 221.8 | 1351292 | 0.2000 |

The output from the Xfoil analysis shows that the effect of the speed on the lift curve slope is to increase the maximum lift coefficient, while all other parameters remain the same. Figure 5.1 and Figure 5.2 show the lift curve slope and the drag polar for the Clark Y airfoil. In addition, Table 5.2 summarizes the results of the Xfoil analysis.

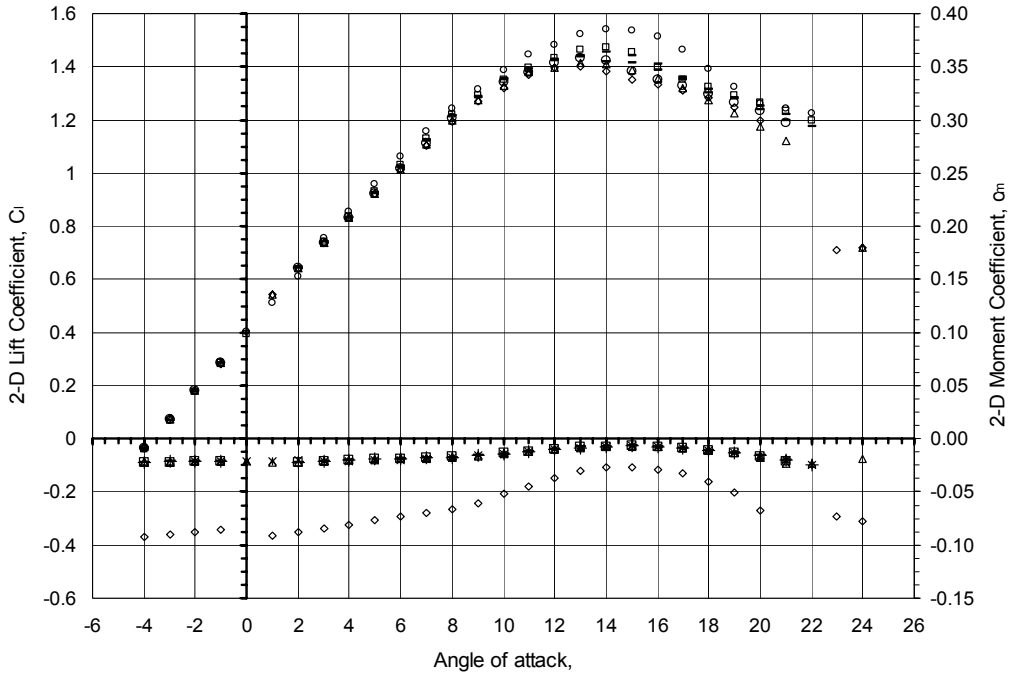


**Figure 5.1**: Lift coefficient vs. angle of attack for the Clark Y airfoil.

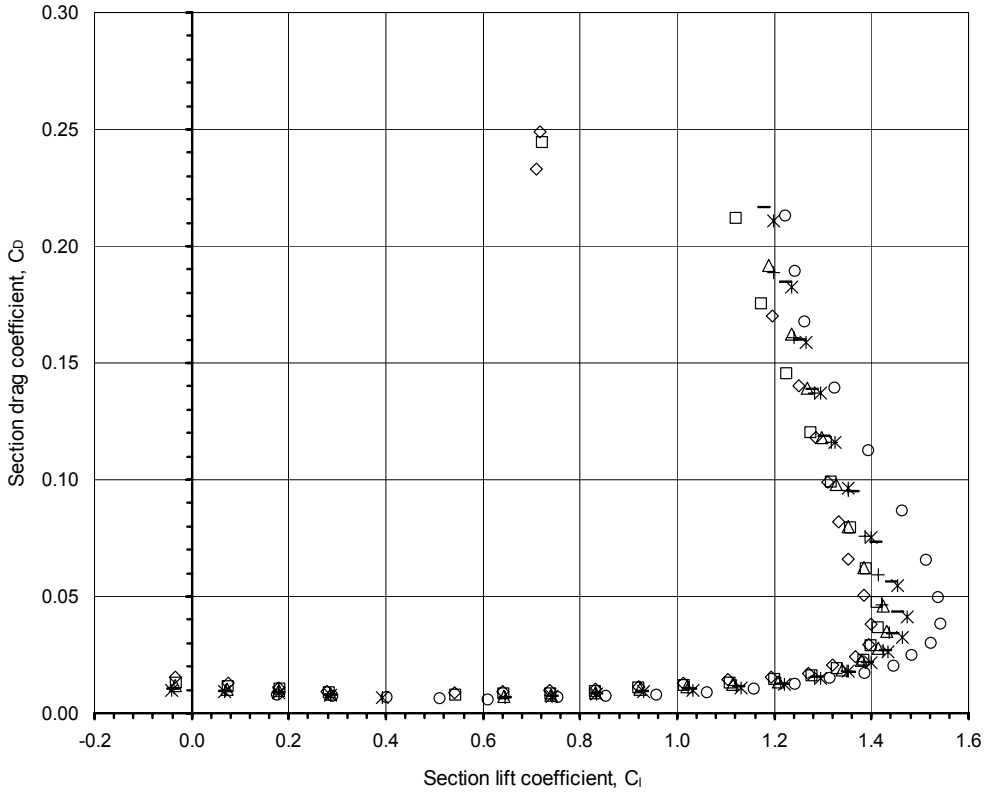


**Figure 5.2:** Drag coefficient vs. lift coefficient.

**Table 5.2:** Summary of Xfoil analysis

Lift curve slope, $(\delta C_l/\delta\alpha)$ = 5.73 per radians

Zero lift angle of attack, $\alpha_{lo}$ = -3.54 degrees

| Velocity (mph) | Velocity (ft/s) | $C_{l\,max}$ | $\alpha_{C\,l\,max}$ (degrees) |
|---|---|---|---|
| 30 | 44.0 | 1.3995 | 13 |
| 40 | 58.7 | 1.4147 | 13 |
| 50 | 73.3 | 1.4325 | 13 |
| 60 | 88.0 | 1.4371 | 13 |
| 70 | 102.7 | 1.4536 | 14 |
| 80 | 117.3 | 1.4725 | 14 |
| 151.2 | 221.8 | 1.5422 | 14 |

## 5.2 Vortex Lattice Simulation

### 5.2.1 Methods for the Definition of the Wing in VLMpc

VLMpc simulates a flow over a body assuming that this body can be represented by its mean surface. In order to determine this mean surface the angles of attack at the control points have to be determined by the user and declared as an input to the program. For wings or body with no camber, all the angles of attack are zero and no special input has to be done by the user. But for a cambered wing these angles have to be determined by the user.

For design purposes we needed to represent the wing body to compute it's aerodynamic properties. In the case of interest in our design, we had to determine these angles of attack to make a good representation of our morphing wing in its different configurations. At this point the only wing changes that were simulated in VLMpc were the flap extensions, and the sweep of the wing flap retracted.

### 5.2.2 Description of the wing body and reference frames

Figure 5.2.1 shows the two reference frames used for this analysis. The first reference frame, *F*:(x, y, z), is the one used to define the geometry of the wing body. In this reference frame the axis coincides with the aircraft center of symmetry, y points toward the tip of the right wing and the z axis points straight downwards. The second reference frame, *W*:($\bar{x}$ , $\bar{y}$ , $\bar{z}$ ), will be used to determine the location of the control point on the wing. The $\bar{y}$ axis will always stay along the leading edge, the $\bar{x}$ axis is oriented perpendicular to the leading edge and $\bar{z}$ points in the same direction as for the z axis in the VLMpc reference frame. The unit of measure in the (x, y, z) reference frame is inches, and in the wing reference frame the chord length is 13". Since the rotation point is located at (-8,-8, 0) in *F*, to go from *F* to *W* the following transformation has to be done:

$$\begin{Bmatrix} \bar{x} \\ \bar{y} \\ \bar{z} \end{Bmatrix} = \begin{bmatrix} \cos\Lambda & -\sin\Lambda & 0 \\ \sin\Lambda & \cos\Lambda & 0 \\ 0 & 0 & 1 \end{bmatrix} \begin{Bmatrix} \frac{x+8}{13} \\ \frac{y+8}{13} \\ \frac{z}{13} \end{Bmatrix} \tag{5.1}$$

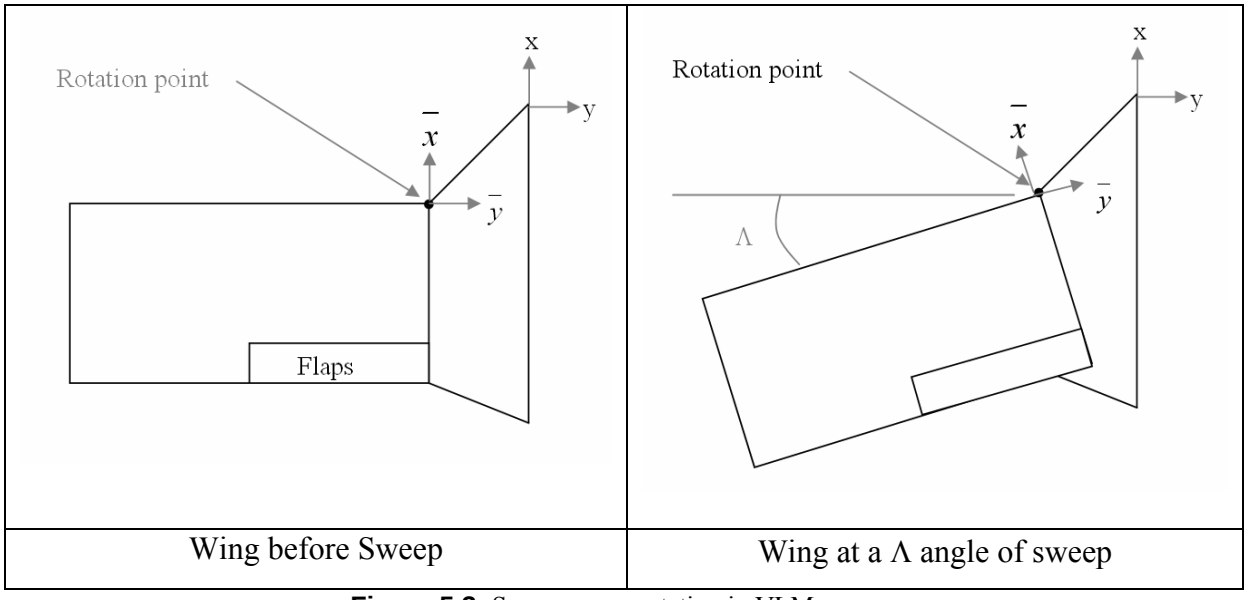


| Wing before Sweep | Wing at a Λ angle of sweep |
|---|---|

**Figure 5.3:** Sweep representation in VLMpc

When simulating the wing body shape in VLMpc we assume that the "body" that is define by the fixed parallelogram has no camber and that the sweeping wing has a

traditional Clark Y camber, with a local (optional) camber modification to represent the flap.

### 5.2.3 Determination of the camber of the Clark Y airfoil

The data that was available for the mean camber line of the Clark Y was a table. In order to be able to determine the local angle of attack at an arbitrary position of the chord a polynomial was computed to summarize the data. To reduce this data and determine the coefficient of the polynomial function "fitcurve10" was written.

```
function c=fitcurve10(oo)

OUT=Datanaca(0);
x=-OUT(:,1);
z=-OUT(:,2);

M=length(z);
A=zeros(M,10)+1;
for i=2:10
    for j=1:M
        A(j,i)=x(j)^(i-1);
    end
end
AT=transpose(A);

c=(AT*A)^-1*AT*z;
```

This function extract the data stored in "datanaca" and fit a 9th order polynomial through this data.
The function returns a "c" vector containing the coefficient of the polynomial.

Then the camber is represented in a function of the form:

$$f(\bar{x}) = \sum_{i=0}^{9} c_i \bar{x}^i \qquad (5.2)$$

### 5.2.4 Definition of the mean surface of wing body in VLMpc

The function describing the surface of the wing body can easily be defined in the *W* reference frame:

$$\bar{z} = f(\bar{x}, \bar{y}) = \begin{cases} \sum_{i=0}^{9} c_i \bar{x}^i & for \quad \bar{y} < 0 \\ 0 & for \quad \bar{y} > 0 \end{cases} \tag{5.3}$$

The cambered surface representing the wing is shown is the following 3d plot:

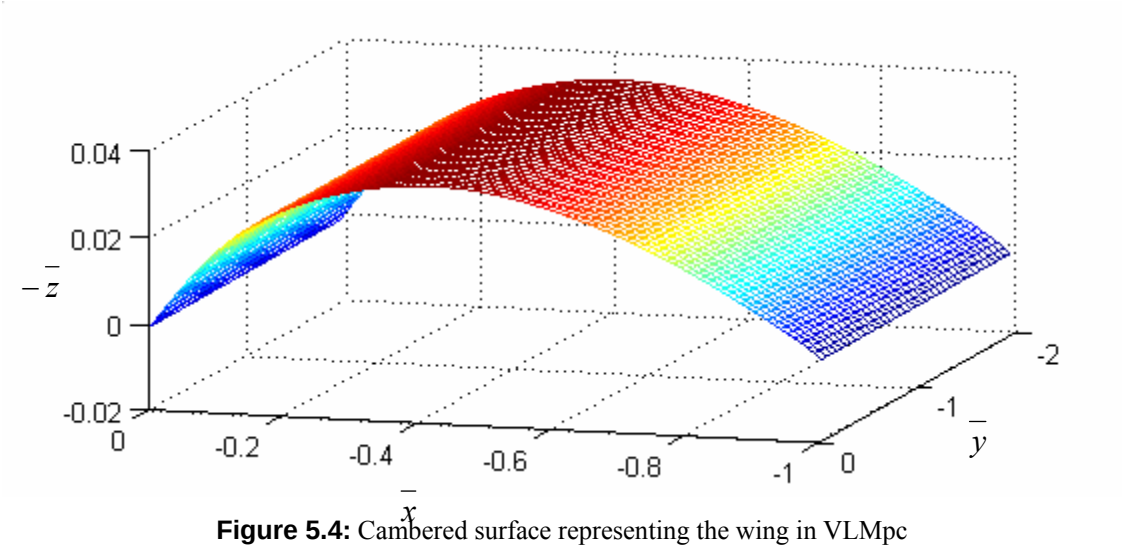


**Figure 5.4:** Cambered surface representing the wing in VLMpc

Note: - In order to show the camber the $\bar{z}$ axis was exaggerated.

- The z axis was inverted to show a positive camber.

In order to determine the local angle of attack, the coordinates in *F* of the control points have to be transformed in coordinates on the *W* reference frame.

### 5.2.5 Measurement of the local angle of attack in the *W* frame

Figure 5.5 represents the camber line of the Clark Y. Using the function in equation (5.2), we can determine the slope of that line:

$$\frac{\partial \bar{z}}{\partial \bar{x}} = f'(\bar{x}) = \sum_{i=0}^{9} ic_i \bar{x}^{(i-1)} \tag{5.4}$$

If we define $\vec{N}$ as the vector normal to the cambered surface then $\vec{N}$ would be defined as:

$$\vec{N} = \nabla\left(f(x,y) - z\right) \tag{5.5}$$

In the *W* referential $\vec{N}$ becomes:

$$\vec{N}_W = \begin{Bmatrix} \frac{\partial f}{\partial \bar{x}} \\ 0 \\ -1 \end{Bmatrix} \tag{5.6}$$

To describe $\vec{N}$ in the *F* reference frame, the following transformation has to be done:

$$\vec{N}_F = 13 \times \begin{bmatrix} \cos(\Lambda) & \sin(\Lambda) & 0 \\ -\sin(\Lambda) & \cos(\Lambda) & 0 \\ 0 & 0 & 1 \end{bmatrix} . \vec{N}_W = \begin{Bmatrix} \frac{\partial f}{\partial \bar{x}} \cos(\Lambda) \\ -\frac{\partial f}{\partial \bar{x}} \sin(\Lambda) \\ -1 \end{Bmatrix} \tag{5.7}$$

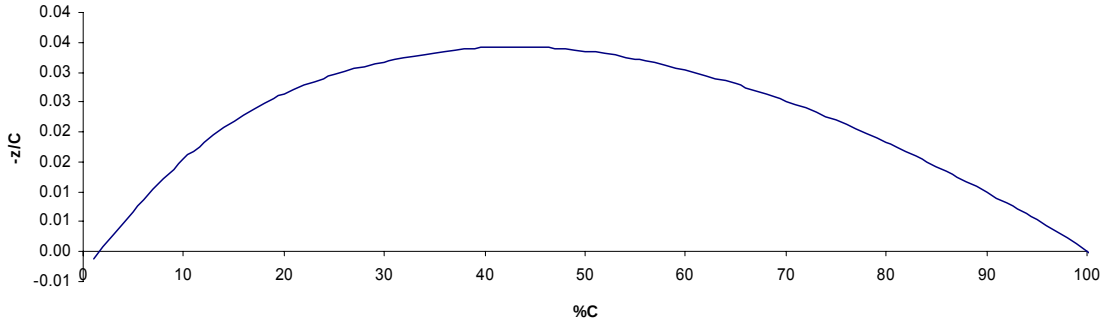


**Figure 5.5.** Mean camber line of Clark Y profile

Figure 5.6 below shows the angle of attack at a given point using the normal vector:

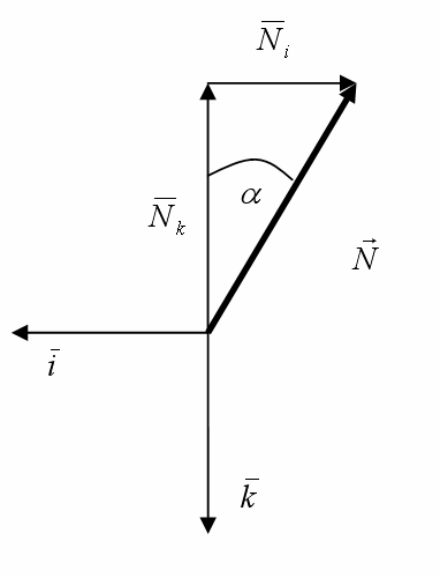


**Figure 5.6.** Vectorial representation of Angles

Therefore the local angle of attack is defined by:

$$\alpha = -\tan^{-1}\left(\frac{\overline{N}_i}{\overline{N}_k}\right) \qquad \text{or} \qquad \alpha = \tan^{-1}\left(-\frac{\partial f}{\partial \bar{x}}\right)$$

$$\alpha\left(\bar{x}\right) = -\tan^{-1}\left(\cos(\Lambda)\times\sum_{i=0}^{9} ic_i\,\bar{x}^{(i-1)}\right) \tag{5.8}$$

### 5.2.6 Presentation of Matlab Functions to Create VLMpc Input File

In order to avoid programming error in the creation of input files, and also to have and automated generator of input file for each configuration, a Matlab routine was written based on the sweep and span extension. The script file used for that purposed was the following:

```
%Set L>0 for Sweep and L<0 for span Extension
%Procedure:
%   -   Set L positive for sweep
%             negative for span extension
%   -   Paste diplay in command window in input file
%       Run VLMpc
%   -   Extract from output VLMpc the coordinates from VLMpc output file
%       Past coordinates for wing in Xw and for tail in Xt
%   -   Hit any key on command window
%       Paste the first set of angles in input file
%       Align manually data before runing
%   -   Run, Save Output file, add completed input in log
%       Replace Tail angles with second series of angle
%   -   Run, Save Output file
%   -   Hit Back twice in this script file to delete coordinate matrices
%   -   Move to next case
clc
clear all
L=45;


Finaldesign(L);



pause

del=5;
Xw=['Copy table for wing control points here'];
Xt=['Copy table for tail control points here'];
angledesign(Xw,Xt,L,del);

%%%%%%%%%%%%%%%%
%     LOG      %
%%%%%%%%%%%%%%%%

%   -   Built from previous program version on April 1st 2005
%   -   Case span retracted 0 sweep 01/04/05
%       Ready to run any case on sweep
%       Ready to run on span extension
%   -   All sweep done
%   -   All Extension done
```

This script has to be executed in two steps because the logic used to place the control points was difficult to reproduce, or in other words it would have been more time consuming to determine and program the logic than just manually input the disposition of control points, from the flat solution output.

This script file calls two functions. The first is “Finaldesign(L)” which will draw the contour of the aircraft based on the input variable L which defines the wing configuration.

```
function L=Finaldesign(eL)
% This function draws the contour of the wing
%To use this function use Script file "Finaldesigncontrol"

%clear all
%clc
%eL=-18;

if eL==0
    L=0;
    ext=0;
elseif eL<0
    L=0;
    ext=-eL;
else
    L=eL;
    ext=0;
end

disp(' ')
disp(sprintf('Morphing Wing, Full flat ac Sweep= %0.0f Ext=%0.1f"',L,ext))
disp('2.        1.        13.       858.      -11.25')


if ext~=0
    disp('12.        0.        0.        0.')
    disp('4.0       0.0       0.0       1.')
    disp('-1.0      -3.0      0.        1.')
    disp('-3.0      -3.0      0.        1.')
    disp('-8.0      -8.0      0.        1.')
    disp('-8.00     -33.00    0.        1.')
    disp('-8.75     -33.00    0.        1.')
    disp(sprintf('-8.75     %0.2f    0.        1.',-33-ext))
    disp(sprintf('-17.45    %0.2f    0.        1.',-33-ext) )
    disp('-17.45    -33.00    0.        1.')
    disp('-21.00    -33.00    0.        1.')
    disp('-21.00    -8.00     0.        1.')
    disp('-26.0     -3.0      0.        1.')
    disp('-26.      0.')
```

```
else
    %%Drawing the edge of Main wing
    disp('8.        0.        0.        0.')

    %Nose
    disp('4.0       0.0       0.0       1.')
    %Eye
    disp('-1.0      -3.0      0.        1.')
    %Neck
    disp('-3.0      -3.0      0.        1.')
    %Shoulder
    disp('-8.0      -8.0      0.        1.')
    %TipLE
    r=25;
    t=(L)*pi/180+pi/2;
    x=r*cos(t)-8;
    y=-r*sin(t)-8;
    if x>-10
        if y>-10
            disp(sprintf('%0.2f     %0.2f     0.        1.',x,y))
        else
            disp(sprintf('%0.2f     %0.2f    0.        1.',x,y))
        end
    else

        if y>-10
            disp(sprintf('%0.2f    %0.2f     0.        1.',x,y))
        else
            disp(sprintf('%0.2f    %0.2f    0.        1.',x,y))
        end
    end


    %TipTE
    r=sqrt(13^2+25^2);
    t=(L+90)*pi/180+atan(13/25);
    D9=r*cos(t);
    E9=r*sin(t);
    y1=r*cos(t)-8;
    x=y1;
    x1=-r*sin(t)-8;
    y=x1;
    if x>-10
        if y>-10
            disp(sprintf('%0.2f     %0.2f     0.        1.',x,y))
        else
            disp(sprintf('%0.2f     %0.2f    0.        1.',x,y))
        end
    else
        if y>-10
            disp(sprintf('%0.2f    %0.2f     0.        1.',x,y))
        else
            disp(sprintf('%0.2f    %0.2f    0.        1.',x,y))
        end
    end
    %disp('Touch')
    r=13;
    t=(L+180)*pi/180;
    D12=r*cos(t);
    E12=r*sin(t);
    y2=r*cos(t)-8;
    x2=-r*sin(t)-8;
    a=(y2-y1)/(x2-x1);
    b=y2-a*x2;
    xt=-(29+b)/(a+1);
    x=-29-xt;
    y=xt;
    if x>-10
        if y>-10
            disp(sprintf('%0.2f     %0.2f     0.        1.',x,y))
        else
            disp(sprintf('%0.2f     %0.2f    0.        1.',x,y))
        end
```

```
    else
        if y>-10
            disp(sprintf('%0.2f    %0.2f     0.        1.',x,y))
        else
            disp(sprintf('%0.2f    %0.2f    0.        1.',x,y))
        end
    end
    %Beltl
    disp('-26.0     -3.0      0.        1.')
    %Belt2
    disp('-26.      0.')
end
%%%Plot the tail
disp('6.        0.        0.        0.')
disp('-26.      -0.       0.        1.')
disp('-26.      -3.       0.        1.')
disp('-48.      -1.5      0.        1.')
disp('-49.75    -15.      0.        1.')
disp('-56.75    -15.      0.        1.')
disp('-58.5     -1.5      0.        1.')
disp('-58.5     0.0       0.        1.')

disp('1.   6.   13.   .05 11.  0.   0.   0.   0.        0.   0.        0.')
```

After the coordinates of the contour were defined, a first input file without the local angles was defined to compute the flat output solutions. The flat solution was used to compute the disposition of the vortex control points. The coordinates of the control points are then used to determine the local angle of attack.

This task is done by the “angledesign(X1,X2,l, del)” function. This function creates the group 3 of the input files using the methods described earlier in this paper.

```
function o=angledesign(X1,X2,l,del)
% Displayed local angle of wing followed of angle of tail at +del
% then display the list of angles for tail at -del.
%To use this function use Script file "Finaldesigncontrol"

disp(' ')
disp('---------------')
disp(' ')

if l<0
    %Span expansion
    disp(sprintf('Morphing Wing, Full ac Sweep= %0.0f del=%0.0f Ext=%0.1f"',0,del,-l))
    outanglext(X1);

else
    %Get angles for main wing
    disp(sprintf('Morphing Wing, Full ac Sweep= %0.0f del=%0.0f Ext=%0.1f"',l,del,0))

    o=outangle(X1,l);
end
```

```
%Make angles for tail
X=[X2(:,3),X2(:,4)];
s=length(X2(:,1));
a=zeros(s,1);
test=a;
d=-del*pi/180;
for i=1:s
    if X(i,1)>-48 %Position on the fuselage
        a(i)=0;
        test(i)=1;
    elseif X(i,2)>-1.5
        a(i)=0;
        test(i)=2;
    else
        a(i)=d;
        test(i)=3;
    end
end
for j=0:length(a)/6-1
    disp(sprintf('%1.5f   %1.5f   %1.5f   %1.5f   %1.5f   %1.5f   ',a(j*6+1),a(j*6+2),a(j*6+3),a(j*6+4),a(j*6+5),a(j*6+6)))
end
disp(' ')
disp('....|....|....|....|....|....|....|....|....|....|....|....|')
disp(' ')

a=zeros(s,1);
d=del*pi/180;
for i=1:s
    if X(i,1)>-48 %Position on the fuselage
        a(i)=0;
        test(i)=1;
    elseif X(i,2)>-1.5
        a(i)=0;
        test(i)=2;
    else
        a(i)=d;
        test(i)=3;
    end
end
for j=0:length(a)/6-1
    disp(sprintf('%1.5f   %1.5f   %1.5f   %1.5f   %1.5f   %1.5f   ',a(j*6+1),a(j*6+2),a(j*6+3),a(j*6+4),a(j*6+5),a(j*6+6)))
end
```

### 5.3 Results and Discussion of VLMpc Simulation

VLMpc provided the project with valuable information about the capability and benefits provided by the morphing design. In the following section of this report, these results are described from two perspectives: Longitudinal stability and aerodynamic performance. The longitudinal stability was an important concern in the development of the morphing wing aircraft. The changes in the span and the sweep of the wing induce large changes on the aerodynamic characteristics of the aircraft. In order to ensure flight stability, a careful analysis of the center of pressure was conducted. This analysis was conducted in two parts. This first part concerns the span extension case, and the second part focuses on the characteristics in sweep. The results will be presented in this report in two distinct parts. The first part will concern the evolution of the aerodynamic characteristics in sweep and the second in span extension.

### 5.3.1 Aerodynamic Characteristics of Aircraft in Span Extension.

***Aerodynamics performance*** The expanded span wing configuration will be used in loiter and short take off (or landing). Since the span can be set to different levels of extension, multiple degrees of extension were simulated in VLMpc. The following table presents the aerodynamic characteristics of the aircraft at these different degrees of extension $\Delta b$:

**Table 5.3:** Aerodynamic characteristics of aircraft in span extension

| Δb | Case1 $\delta_{HT}$ | Case2 $\delta_{HT}$ | $CL_\alpha$ | | CL Twist | $\alpha_{0L}$ | $y_{CP}$ | Cm/CL | Case1 $Cm_{0L}$ | Case2 $Cm_{0L}$ |
|---|---|---|---|---|---|---|---|---|---|---|
| | | | per Rad | per Deg | | | | | | |
| 0 | 5 | -5 | 4.88226 | 0.08521 | 0.10756 | -1.26229 | -0.41553 | -0.23858 | 0.2297 | -0.22278 |
| 3 | 5 | -5 | 5.40338 | 0.09431 | 0.11898 | -1.26166 | -0.41409 | -0.23013 | 0.22879 | -0.22593 |
| 6 | 5 | -5 | 5.89764 | 0.10293 | 0.12832 | -1.24659 | -0.41207 | -0.22622 | 0.23704 | -0.22523 |
| 9 | 5 | -5 | 6.36604 | 0.11111 | 0.13401 | -1.20614 | -0.41001 | -0.21737 | 0.23578 | -0.2283 |
| 12 | 5 | -5 | 6.84485 | 0.11947 | 0.1306 | -1.09318 | -0.40827 | -0.21045 | 0.24057 | -0.24034 |
| 15 | 5 | -5 | 7.28462 | 0.12714 | 0.13507 | -1.06234 | -0.40666 | -0.20191 | 0.23969 | -0.24301 |
| 18 | 5 | -5 | 7.72003 | 0.13474 | 0.13938 | -1.03443 | -0.40576 | -0.19381 | 0.2388 | -0.2458 |
| 18.5 | 5 | -5 | 7.79049 | 0.13597 | 0.13953 | -1.02616 | -0.40566 | -0.19253 | 0.23875 | -0.24617 |

Using the results shown in the table above and assuming that the maximum lift is provided at $12^o$, the lifting capability of the aircraft is shown in Figure 5.7.

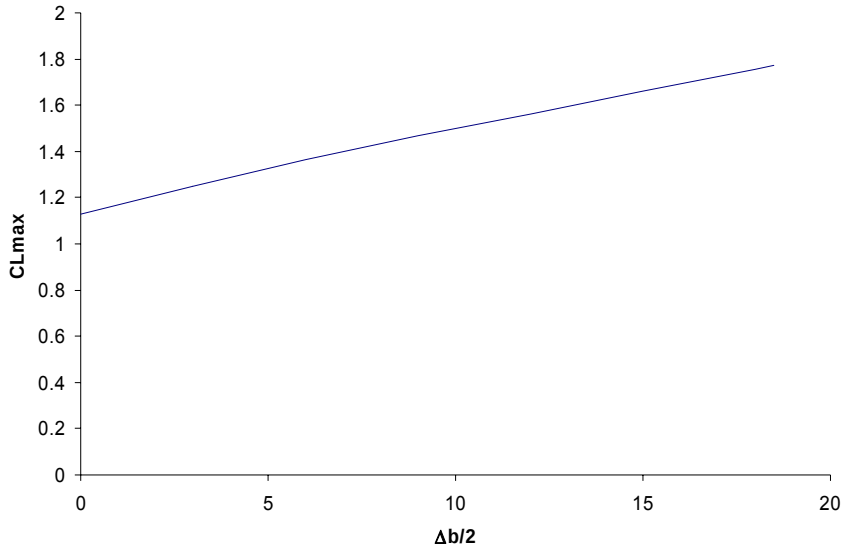


**Figure 5.7: Lifting capability in span extension**

The span extension increases the maximum lift available from 1.13 to 1.77, which represents an increase of almost 57%. A great benefit is also observed on the drag

characteristics. Figure 5.8 illustrates this benefit by showing the polar curves for both the retracted and extended case. This figure shows the lift and drag for an angle of attack varying between their respective $\alpha_{0L}$ and 12°. This figure was drawn using a drag estimation for the fuselage of 0.02.

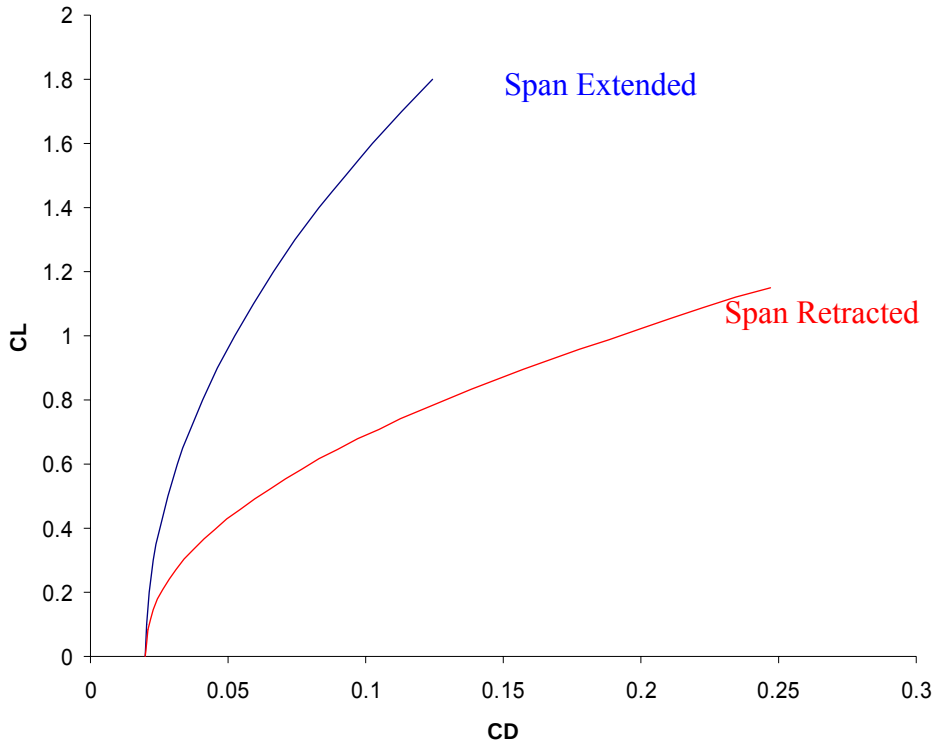


**Figure 5.8:** Polar curves for retracted and extended configuration

This polar curve shows a large increase in *CL/CD*. The max CL/CD in span retracted configuration is increased from 8.9 to 19.7 which is an improvement by more than 100%.

***Longitudinal stability*** As the span is extended the $C_{M\,0}$ of the main wing tends to decrease, inducing a nose down moment. This nose down moment moves the neutral point forward. This phenomenon is shown in Figure 5.9. The full span out configuration will be the unstable limit of the aircraft.

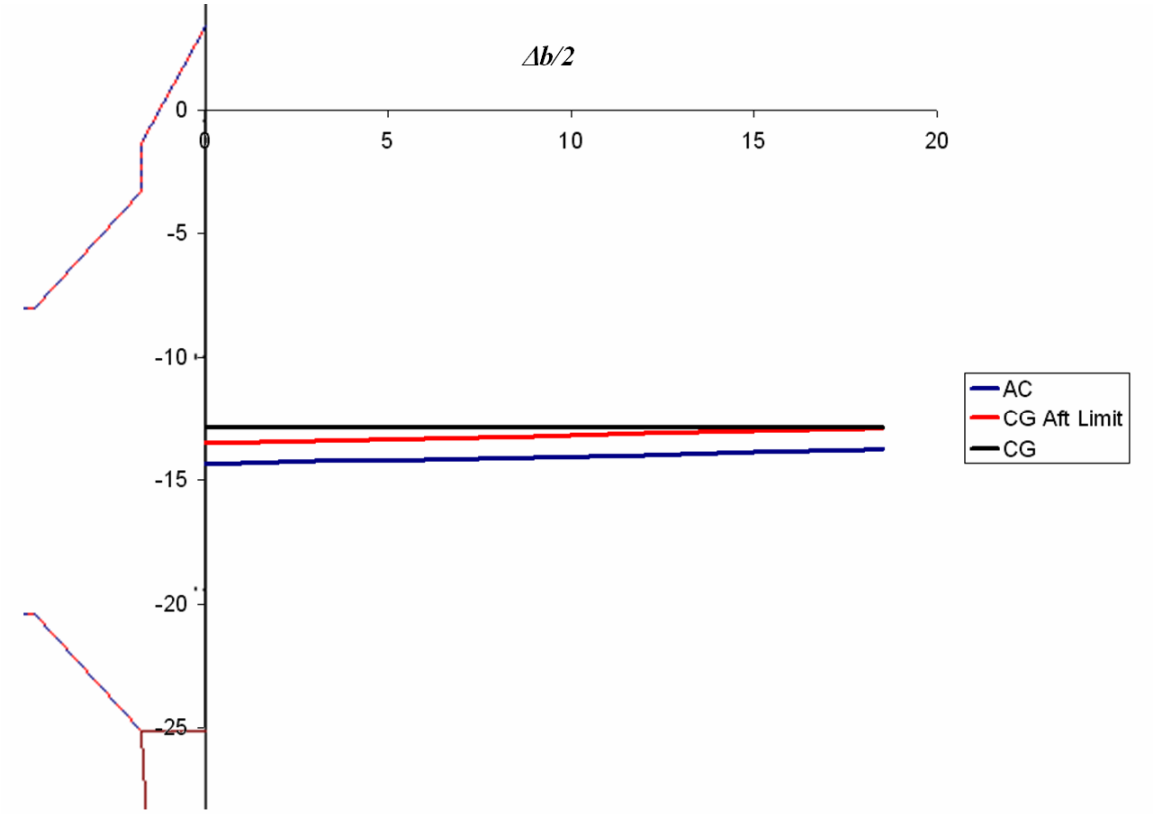


**Figure 5.9:** Longitudinal stability in loiter configuration

During the process of extending the span, wing elements are moving laterally. The longitudinal position of the center of gravity CG remains unchanged. Since 5% static margin is assumed to be "reasonable" as long as the CG longitudinal position remains fore by 12.9" in the aircraft reference frame, the span out configuration will be satisfactorily stable. In Figure 5.10, we can see the evolution of the static margin in span extension.

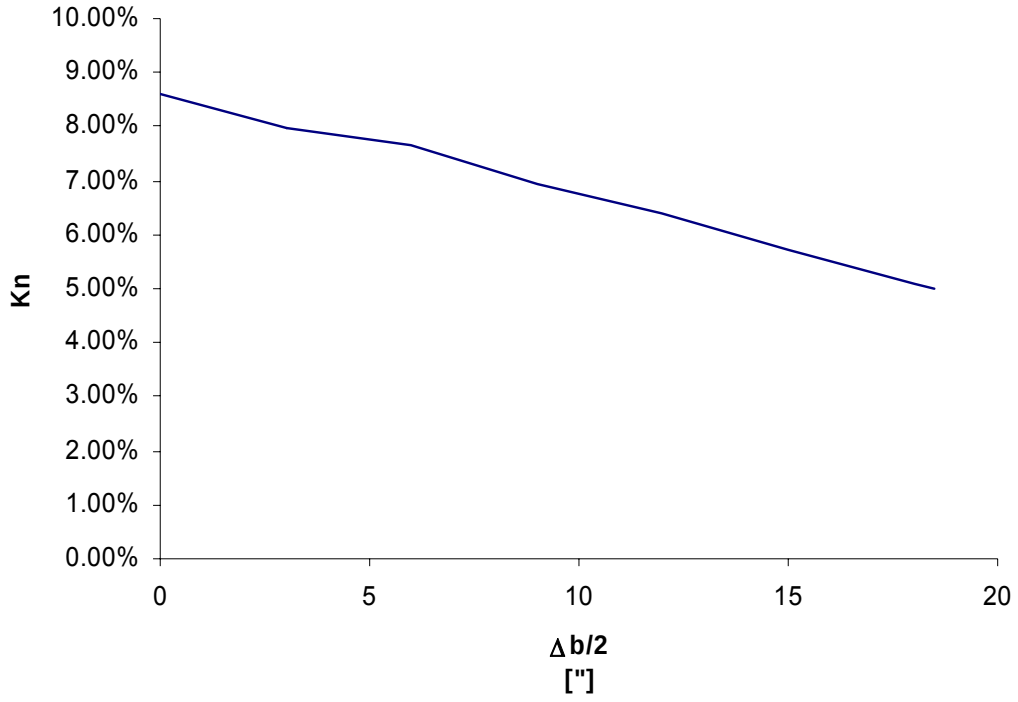


**Figure 5.10:** Static Margin evolution during span extension

We can see in Figure 5.10 that the evolution of the static margin is smooth and should not drastically affect the handling quality of the aircraft. The fact that the span extension decreases the static margin, it might be hazardous to attempt to fly both in chord extended (flaps down) and span extended without a careful investigation of the effect of flaps on stability.

### 5.3.2 Aerodynamic Characteristics of Aircraft in Sweep

***Aerodynamics performance*** The VLMpc simulation generated the following aerodynamic characteristics for the aircraft in sweep shown in Table 5.3.

**Table 5.3:** Aerodynamic characteristics of aircraft in sweep

| Λ | Case1 $\delta_{HT}$ | Case2 $\delta_{HT}$ | $CL_\alpha$ | | CL Twist | $\alpha_{0L}$ | $y_{CP}$ | Cm/CL | Case1 $Cm_{0L}$ | Case2 $Cm_{0L}$ |
|---|---|---|---|---|---|---|---|---|---|---|
| | | | per Rad | per Deg | | | | | | |
| 0 | 5 | -5 | 4.88226 | 0.08521 | 0.10756 | -1.26229 | -0.41553 | -0.23858 | 0.2297 | -0.22278 |
| 5 | 5 | -5 | 4.8334 | 0.08436 | 0.09482 | -1.12403 | -0.41351 | -0.29114 | 0.22163 | -0.22193 |
| 10 | 5 | -5 | 4.76301 | 0.08313 | 0.08611 | -1.03582 | -0.4127 | -0.3433 | 0.22844 | -0.20587 |
| 15 | 5 | -5 | 4.6629 | 0.08138 | 0.06816 | -0.83758 | -0.41257 | -0.39523 | 0.22338 | -0.20143 |
| 20 | 5 | -5 | 4.52045 | 0.0789 | 0.05403 | -0.6848 | -0.41053 | -0.4473 | 0.21872 | -0.19649 |
| 25 | 5 | -5 | 4.36372 | 0.07616 | 0.03824 | -0.50211 | -0.41081 | -0.49785 | 0.22066 | -0.18528 |
| 30 | 5 | -5 | 4.15922 | 0.07259 | 0.01879 | -0.25883 | -0.40919 | -0.54533 | 0.21812 | -0.17941 |
| 35 | 5 | -5 | 3.9445 | 0.06884 | 0.00047 | -0.00679 | -0.40984 | -0.59067 | 0.21954 | -0.17044 |
| 40 | 5 | -5 | 3.70296 | 0.06463 | -0.01718 | 0.26589 | -0.40879 | -0.62467 | 0.23157 | -0.15835 |
| 45 | 5 | -5 | 3.41275 | 0.05956 | -0.03315 | 0.55659 | -0.40856 | -0.65134 | 0.23902 | -0.14246 |

The changes in aerodynamic characteristics of the wing in sweep are drastic. Significant amount of study was spent to determine these changes and their impact on handling characteristics. This first important change in aerodynamic characteristic was the changes in lift. The Figure bellow presents the decrease in slope of the $CL_\alpha$ as the wing sweeps back.

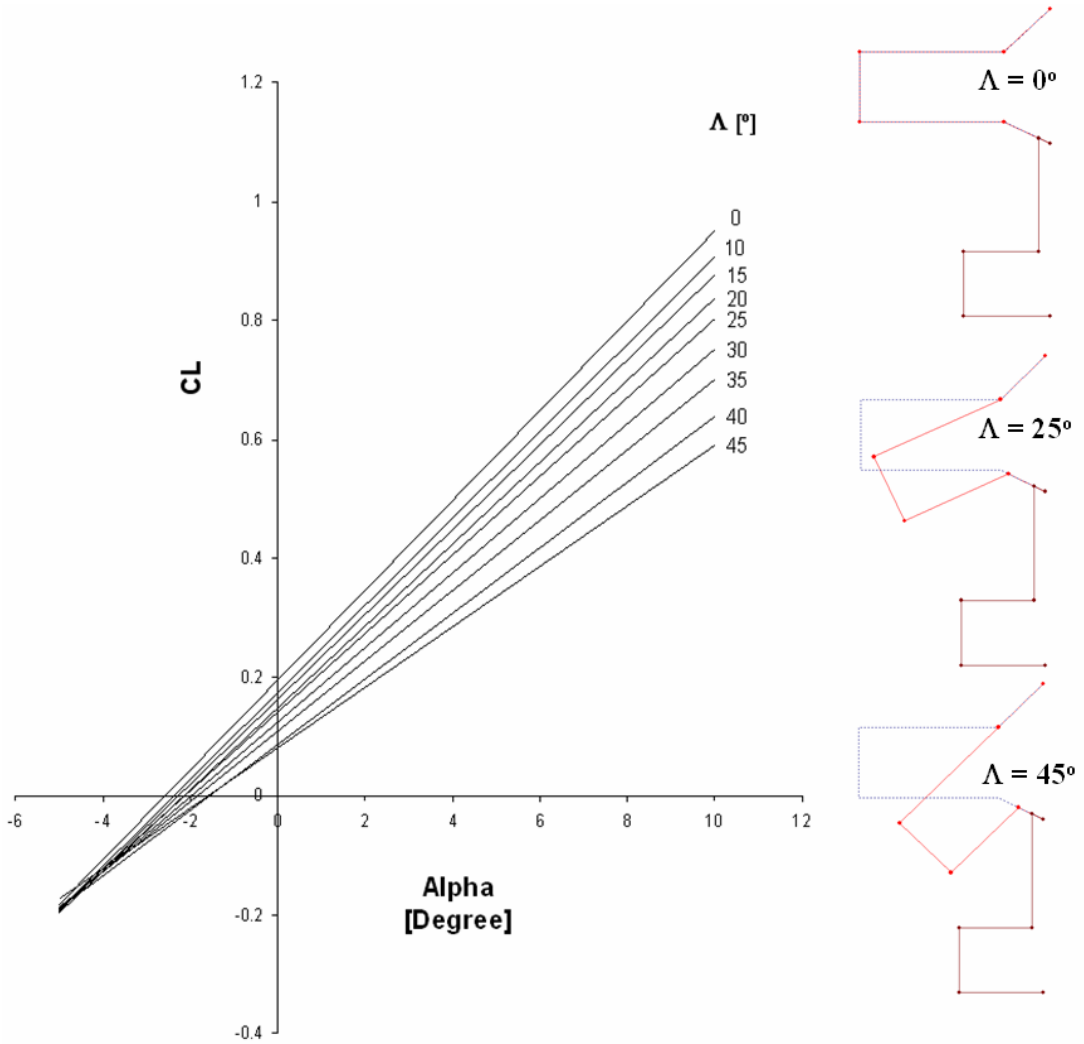


**Figure 5.11:** Lift Coefficient versus α in sweep

The sweep angle also has an impact on $\alpha_0$. The combined effect of the decreasing slope and decreasing $\alpha_0$, drastically reduces the range of lift that can be made available to fly.

Figure 5.12 highlights the drastic decrease in lifting capacity of the aircraft in sweep. Since this configuration is designed for high speed flight situations, lower *CL*s are required.

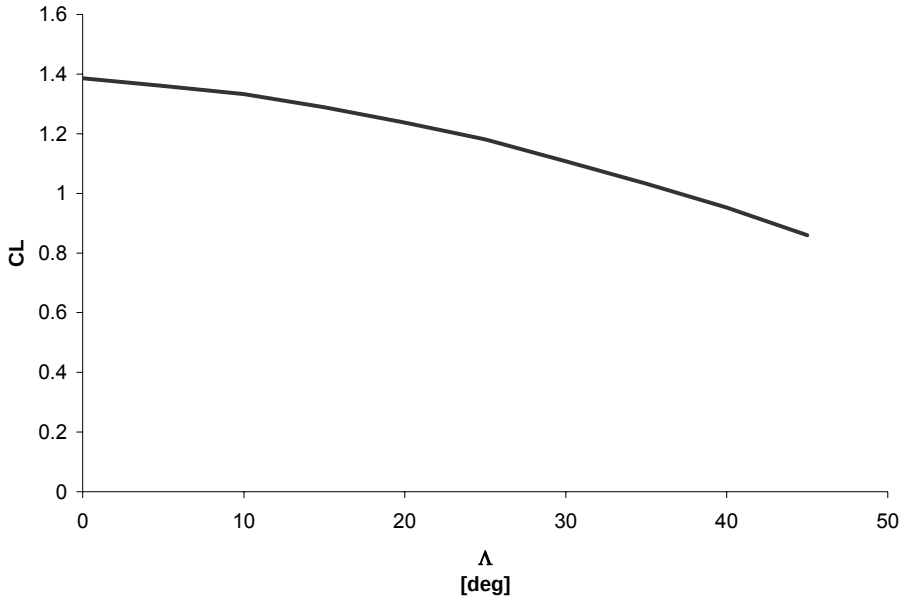


**Figure 5.12:** Maximum CL available as a function of sweep

***Longitudinal stability*** It is challenging to obtain good longitudinal stability characteristics from a variable sweep aircraft. It is challenging because it involves displacements of both the aerodynamic center and the center of gravity.

To simulate the movement of the center of gravity, the mass of the aircraft was separated into two elements:

- The fuselage mass (and its center of gravity) that was induced by the fuselage including the tail, the fuselage structure, and the non-rotating parts of the wing (like the wing shoulders).
- The Wing mass (and its center of gravity) constituted of the mass in the main wing, and the wing extension (in the retracted position).

Figure 5.13 representing the aircraft shows the aircraft and the two mass elements described above.

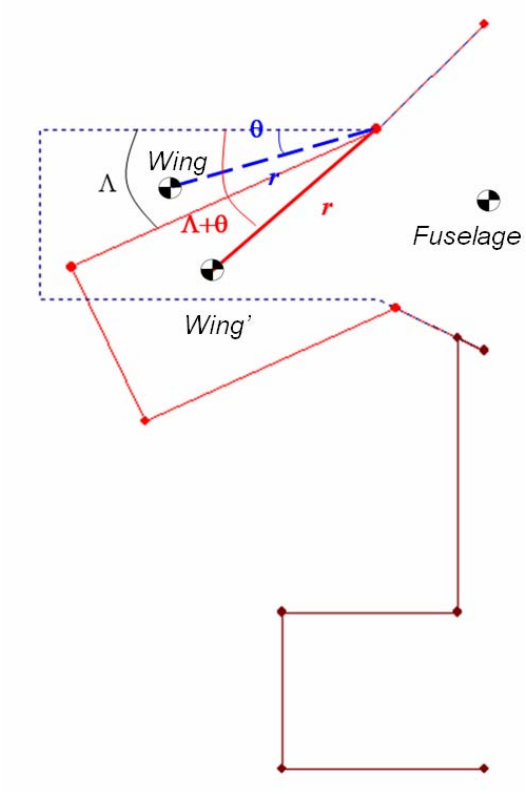


**Figure 5.13:** CG movements diagram

The longitudinal position of the overall CG is determined by the following equation:

$$x_{cg}(\Lambda) = \frac{x_{fuselage} \times m_{fuselage}}{m_{total}} + \frac{\left[x_{w0} + r\left(\sin(\Lambda+\theta) - \sin(\theta)\right)\right] \times m_{wing}}{m_{total}} \tag{5.9}$$

The values of *r* and *h* were estimated using worst case estimates. The initial CG location was determined using the span extended stability limit. Using Equation 5.9, and the aerodynamic results from the VLMpc simulation, the following stability characteristics were defined by Table 5.4:

**Table 5.4:** Stability Characteristics of the aircraft in wing sweep

| Λ | $C_{aero}$ | xac | $CM_\delta$ | $CM_0$ | $x_{cg}$ | Kn | $CM_{CL}$ |
|---|---|---|---|---|---|---|---|
| 0 | 16.8 | -14.35154 | 0.045248 | 0.00346 | -12.9 | 0.086401 | -0.111657 |
| 5 | 16.54 | -15.03482 | 0.044356 | -0.00015 | -13.08834 | 0.117683 | -0.149729 |
| 10 | 16.35 | -15.7129 | 0.043431 | 0.011285 | -13.26196 | 0.149904 | -0.188533 |
| 15 | 16.21 | -16.38799 | 0.042481 | 0.010975 | -13.41956 | 0.183124 | -0.228341 |
| 20 | 16.8 | -17.0649 | 0.041521 | 0.011115 | -13.55991 | 0.20863 | -0.269615 |
| 25 | 16.54 | -17.72205 | 0.040594 | 0.01769 | -13.68196 | 0.244261 | -0.310776 |
| 30 | 16.35 | -18.33929 | 0.039753 | 0.019355 | -13.78479 | 0.278563 | -0.350346 |
| 35 | 16.21 | -18.92871 | 0.038998 | 0.02455 | -13.8676 | 0.312222 | -0.389317 |
| 40 | 16.5 | -19.37071 | 0.038992 | 0.03661 | -13.92976 | 0.329755 | -0.418535 |
| 45 | 16.8 | -19.71742 | 0.038148 | 0.04828 | -13.97081 | 0.34206 | -0.442047 |

The coefficient above represents the influence on the pitching moment of the *CL* (or angle of attack which is directly proportional to *CL*) and the tail deflection $\delta$.
The full equation of the pitching moment can then be defined as:

$$CM(CL,\delta) = CM_\delta \times \delta + CM_{CL} \times CL + CM_0 \tag{5.10}$$

The static marking *Kn* is derived using the mean aerodynamic chord $\bar{c}$:

$$Kn = \frac{x_{ac} - x_{cg}}{\bar{c}} \tag{5.11}$$

Figure 5.14 presents displacements of the AC and of the CG during sweep. These displacements are generated by the physical rotation of the wing in sweep. The aerodynamic influence of the wing on the aircraft is more important than its influence on the weight, the amplitude of displacement of the AC is greater than the one of the CG. This phenomenon induces the increase in the static margin of the aircraft as presented in Figure 5.15.

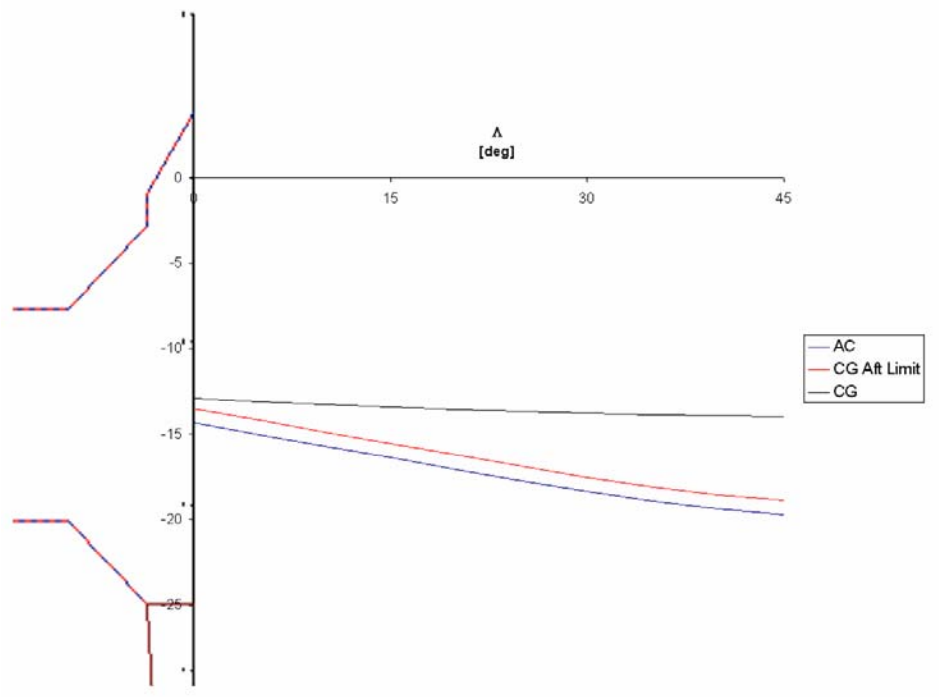


**Figure 5.14:** Displacement of CG and AC

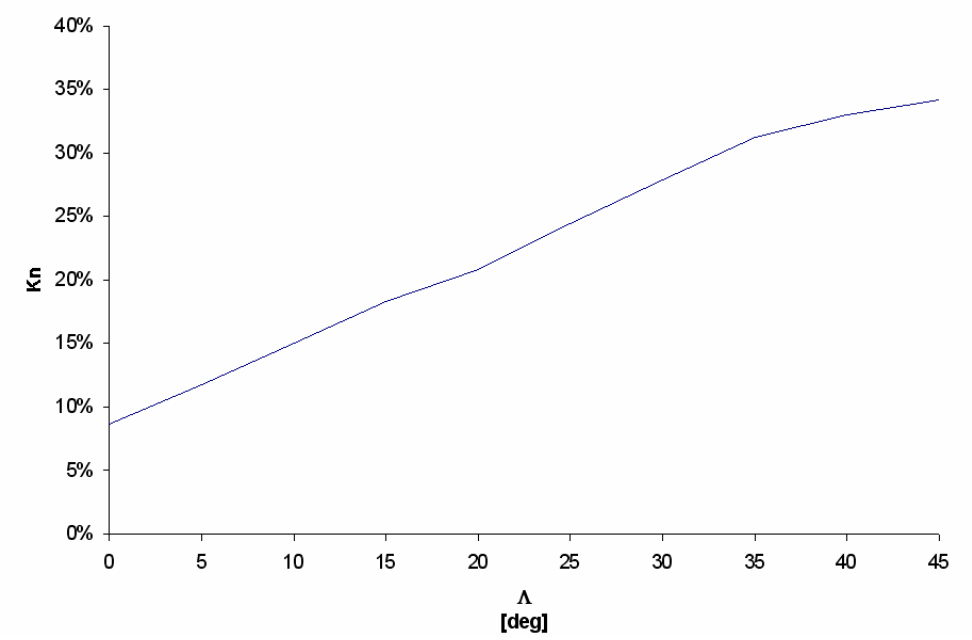


**Figure 5.15:** Static Margin evolution in sweep

Figure 5.15 presents the steady increase in static margin of the aircraft as sweep angle increases. This augmentation is due to the rate of displace of the AC and CG. As a result the level arm between the CG and the point of application of the wing lift (center of

pressure) is increased. This increase will have to be counteracted by the stabilizer (the horizontal tail).

This static margin increase could be lowered from previous design (or from other existing aircraft like the F-111 and F-14) using two factors:

- The outboard position of the pivot point
- The mass distribution between the fuselage and the wing.

The outboard position of the pivot allowed lowering wing surface to be rotated. The fact that a greater proportion of the lifting surfaces were "static" during the rotation decreased the amplitude of AC displacement.

The fact that a greater proportion of mass was located in the wing (compared to F-111 or F-14) was inherent to the material chosen for the construction and to the design complexity of the wing (due to the span and chord extension systems). As a result, 27% of the mass is located in the wing. This fact becomes a great advantage for stability in sweep. A greater proportion of the mass being located in the wing increases the CG shift as the wing is swept.

An alternative that was considered to lower the static margin in sweep was to use a mass correction. This solution would have been implemented as a mass moving aft as the wing is swept. This correction would have increased the shift in CG, therefore decreasing the distance for the AC. This solution was not implemented to the final design because the need was not strong enough.

# Appendix A: Supplemental Construction Drawings

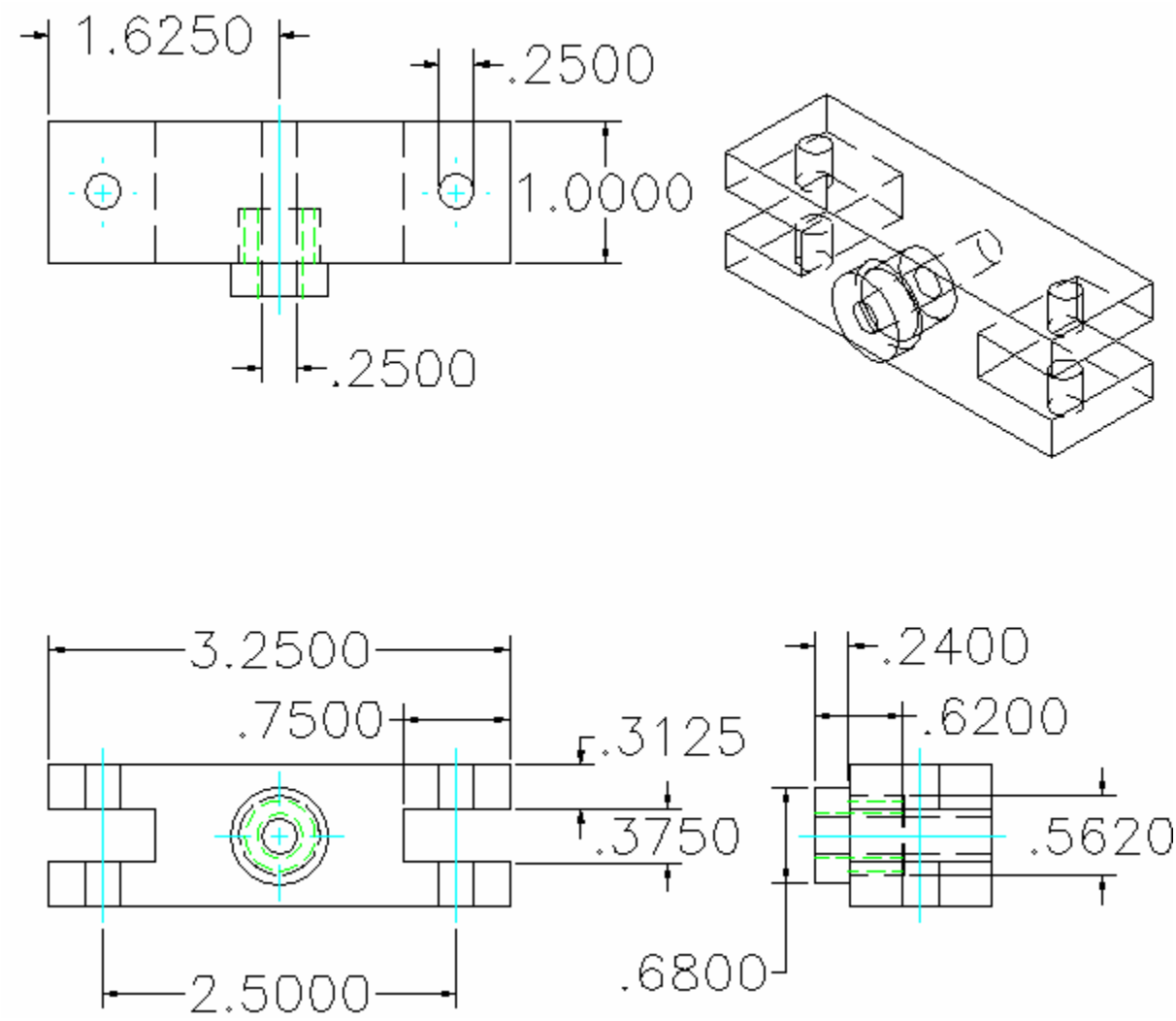


**Figure A-1.** Dimensioned AutoCAD drawing of sweep block. All specified dimensions are in inches.

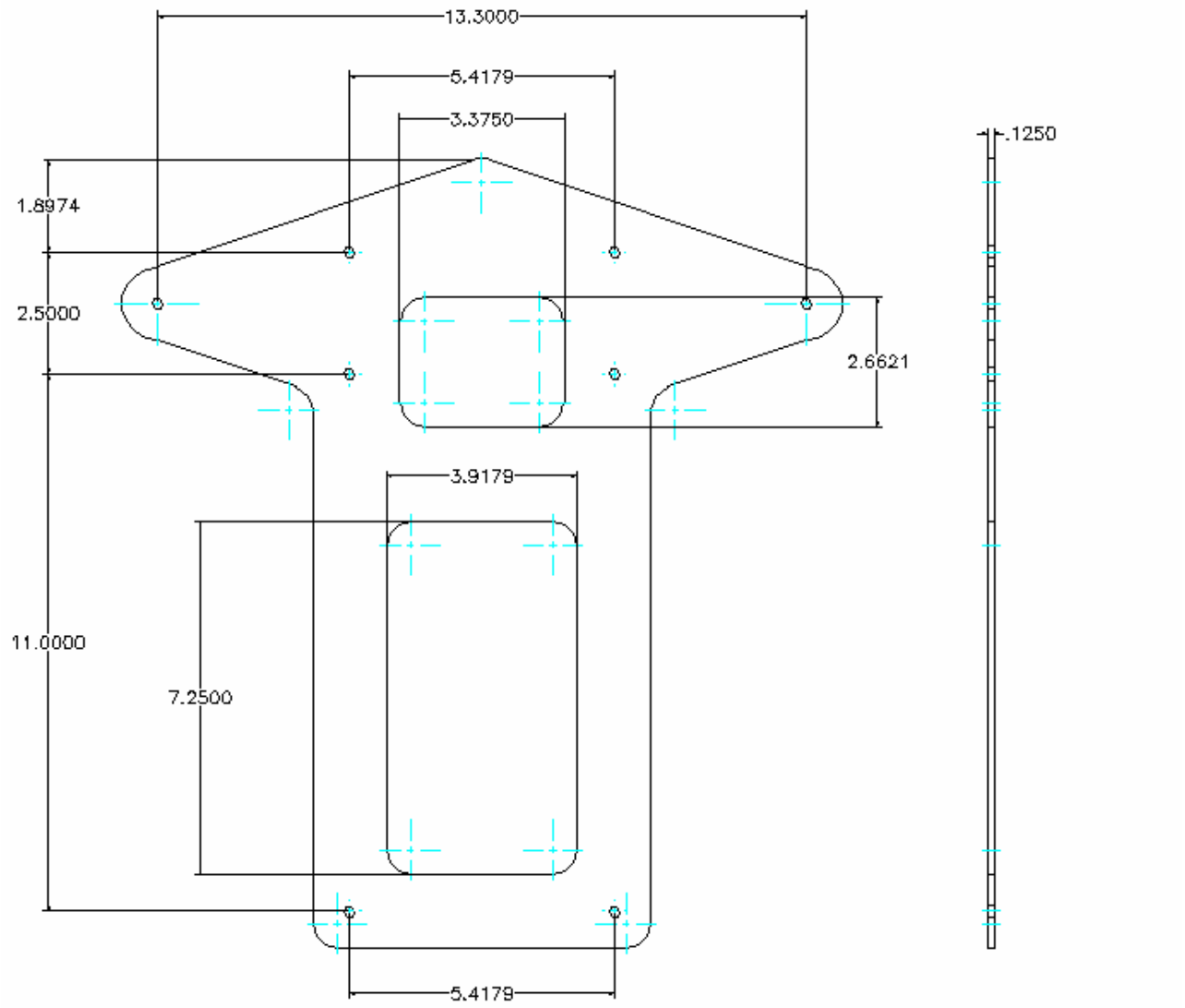


**Figure A-2.** Dimensioned AutoCAD drawing of wing box. All specified dimensions are in inches.

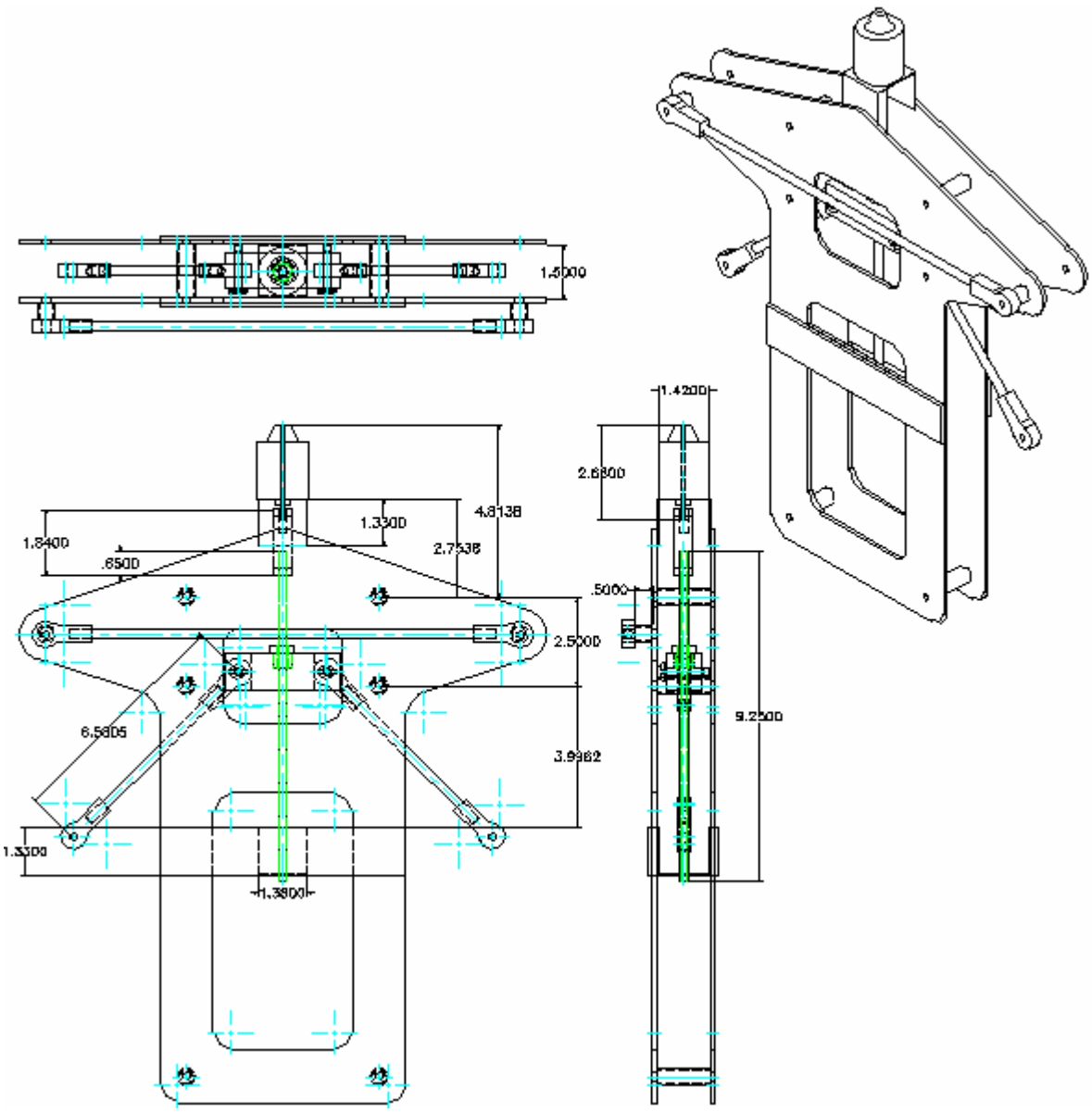


**Figure A-3.** Dimensioned AutoCAD drawing of sweep mechanism. All specified dimensions are in inches.

# Appendix B: Weight Estimation and Clark-Y Tables and Graphs

**Table B-1.** Propulsion weight estimation

| | |
|---|---|
| TOTAL (ozs) | 58.4 |
| (lbs) | 3.65 |

| COMPONENT | QUANTITY | COMPONENT WEIGHT, oz | TOTAL WEIGHT, oz |
|---|---|---|---|
| Engine | 1 | 19.42 | 19.42 |
| Muffler | 1 | 4.88 | 4.88 |
| Engine Mount | 1 | 4.10 | 4.1 |
| Fuel tank | 1 | 5 | 5 |
| Fuel | 1 | 16 | 16 |
| Mounting hardware* | 1 | 5 | 5 |
| Propeller* | 1 | 4 | 4 |

**Table B-2.** Radio control weight

| | |
|---|---|
| TOTAL (ozs) | 18.2 |
| (lbs) | 1.13 |

| COMPONENT | QUANTITY | COMPONENT WEIGHT, oz | TOTAL WEIGHT, oz |
|---|---|---|---|
| Receiver | 1 | 1.75 | 1.75 |
| Receiver Battery | 1 | 3.5 | 3.5 |
| Receiver Power Switch* | 1 | 0.5 | 0.5 |
| Flight control servos | | | |
| Rudder | 1 | 1.3 | 1.3 |
| Elevator | 2 | 1.3 | 2.6 |
| Throttle | 1 | 1.3 | 1.3 |
| Aileron servo | 2 | 1.3 | 2.6 |
| Flap Servo | 2 | 1.3 | 2.6 |
| Nose wheel steering | 1 | 1.3 | 1.3 |
| Foam Padding* | 1 | 0.7 | 0.7 |

**Table B-3.** Landing gear weight

| | |
|---|---|
| TOTAL (ozs) | 22.5 |
| (lbs) | 1.41 |

| COMPONENT | QUANTITY | COMPONENT WEIGHT, oz | TOTAL WEIGHT, oz |
|---|---|---|---|
| Wheels | | | |
| Nose wheel | 1 | 1.5 | 1.5 |
| Main wheels | 2 | 2 | 4 |
| Landing gear | | | |
| Nose gear* | 1 | 6 | 6 |
| Main gear* | 1 | 7 | 7 |
| Mounting hardware* | 1 | 4 | 4 |

**Table B-4.** Actuation system weight

| | |
|---|---|
| TOTAL (ozs) | 24.5 |
| (lbs) | 1.53 |

| COMPONENT | QUANTITY | COMPONENT WEIGHT, oz | TOTAL WEIGHT, oz |
|---|---|---|---|
| Sweep change | n/a | 10 | 10.0 |
| Span change | n/a | 8 | 8.0 |
| Power supply | n/a | 6.5 | 6.5 |

**Table B-5.** Wing weight

| | |
|---|---|
| TOTAL (ozs) | 58.0 |
| (lbs) | 3.63 |

| COMPONENT | QUANTITY | COMPONENT WEIGHT, oz | TOTAL WEIGHT, oz |
|---|---|---|---|
| Structural weight* | 1 | 48 | 48.0 |
| Covering materials* | 1 | 8 | 8.0 |
| Linkages* | 1 | 2.0 | 2.0 |

**Table B-6.** Fuselage and tail weight

| | |
|---|---|
| TOTAL (ozs) | 25.0 |
| (lbs) | 1.56 |

| COMPONENT | QUANTITY | COMPONENT WEIGHT, oz | TOTAL WEIGHT, oz |
|---|---|---|---|
| Structural weight* | 1 | 16 | 16 |
| Covering materials* | 1 | 6 | 6 |
| Linkages* | 1 | 3 | 3 |

## B.2 Properties of the Clark-Y airfoil

**Table B-7.** Clark-Y airfoil coordinates

| x/c | y/c upper | y/c lower |
|---|---|---|
| 0.0000 | 0.0000 | 0.0000 |
| 0.0005 | -0.0047 | 0.0023 |
| 0.0010 | -0.0059 | 0.0037 |
| 0.0020 | -0.0078 | 0.0058 |
| 0.0040 | -0.0105 | 0.0089 |
| 0.0080 | -0.0143 | 0.0137 |
| 0.0120 | -0.0170 | 0.0179 |
| 0.0200 | -0.0203 | 0.0254 |
| 0.0300 | -0.0226 | 0.0330 |
| 0.0400 | -0.0245 | 0.0391 |
| 0.0500 | -0.0260 | 0.0443 |
| 0.0600 | -0.0271 | 0.0488 |
| 0.0800 | -0.0285 | 0.0564 |
| 0.1000 | -0.0294 | 0.0630 |
| 0.1200 | -0.0300 | 0.0686 |
| 0.1400 | -0.0302 | 0.0734 |
| 0.1600 | -0.0303 | 0.0776 |
| 0.1800 | -0.0300 | 0.0811 |
| 0.2000 | -0.0297 | 0.0839 |
| 0.2200 | -0.0291 | 0.0861 |
| 0.2400 | -0.0285 | 0.0878 |
| 0.2600 | -0.0278 | 0.0891 |
| 0.2800 | -0.0271 | 0.0900 |
| 0.3000 | -0.0263 | 0.0907 |
| 0.3200 | -0.0256 | 0.0912 |
| 0.3400 | -0.0248 | 0.0915 |
| 0.3600 | -0.0241 | 0.0916 |
| 0.3800 | -0.0234 | 0.0915 |
| 0.4000 | -0.0226 | 0.0912 |
| 0.4200 | -0.0219 | 0.0906 |
| 0.4400 | -0.0211 | 0.0897 |
| 0.4600 | -0.0204 | 0.0886 |
| 0.4800 | -0.0197 | 0.0874 |
| 0.5000 | -0.0190 | 0.0859 |
| 0.5200 | -0.0182 | 0.0842 |
| 0.5400 | -0.0175 | 0.0824 |
| 0.5600 | -0.0168 | 0.0803 |
| 0.5800 | -0.0160 | 0.0781 |
| 0.6000 | -0.0153 | 0.0758 |
| 0.6200 | -0.0146 | 0.0732 |
| 0.6400 | -0.0138 | 0.0705 |
| 0.6600 | -0.0131 | 0.0676 |
| 0.6800 | -0.0124 | 0.0646 |
| 0.7000 | -0.0116 | 0.0614 |
| 0.7200 | -0.0109 | 0.0582 |
| 0.7400 | -0.0101 | 0.0548 |
| 0.7600 | -0.0094 | 0.0513 |
| 0.7800 | -0.0087 | 0.0476 |
| 0.8000 | -0.0079 | 0.0439 |
| 0.8200 | -0.0072 | 0.0400 |
| 0.8400 | -0.0065 | 0.0361 |
| 0.8600 | -0.0057 | 0.0320 |
| 0.8800 | -0.0050 | 0.0278 |
| 0.9000 | -0.0043 | 0.0235 |
| 0.9200 | -0.0035 | 0.0191 |
| 0.9400 | -0.0028 | 0.0146 |
| 0.9600 | -0.0021 | 0.0100 |
| 0.9700 | -0.0017 | 0.0077 |
| 0.9800 | -0.0013 | 0.0053 |
| 0.9900 | -0.0010 | 0.0030 |
| 1.0000 | 0.0000 | 0.0000 |

**Table B-8.** Geometric properties of the Clark-Y airfoil

| Chord | *c* |
|---|---|
| Maximum camber | 0.03435 *c* |
| Location of max camber | 0.42 *c* |
| Maximum thickness | 0.117 *c* |
| Location of max thickness | 0.29 *c* |
| Circumference | 2.04 *c* |
| Circumference to Chord ratio | 2.04 *c* |

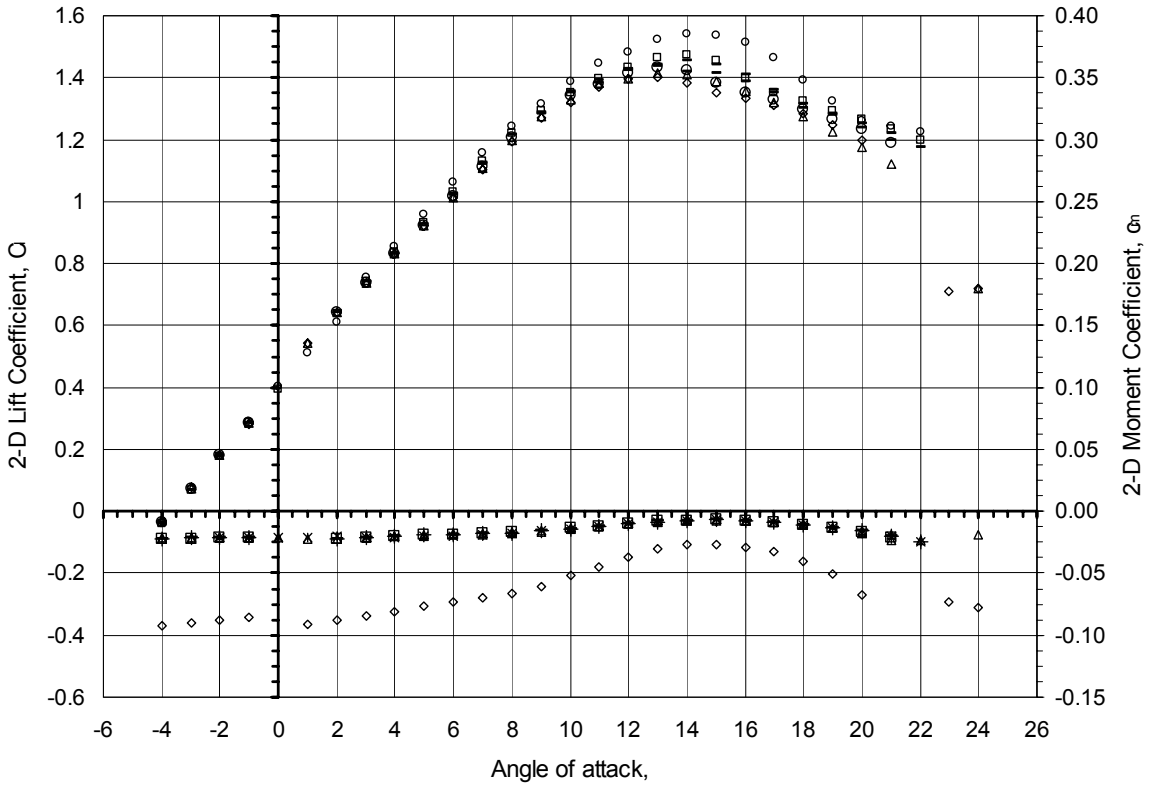


**Figure B-1.** 2-D Lift and pitching moment curves for the Clark-Y airfoil

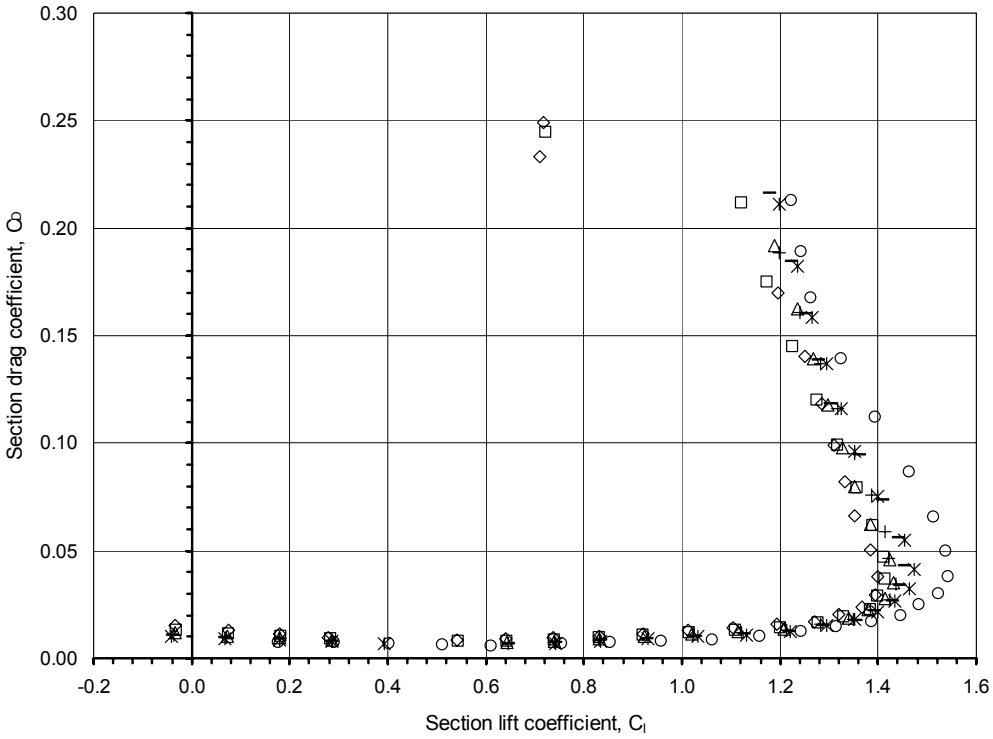


**Figure B-2.** Clark-Y airfoil 2-D Polar curve

## References

**Ref.2.1.** W. H. Mason. *Aero/Hydrodynamics Testing*. AOE 3054 - experiment 7 lab manual. Virginia Tech, 2002.

**Ref.2.2.** M. Leng & C. de Tenorio. *Experimental study of the longitudinal aerodynamic characteristics of six wing models*, 2004.

**Ref.2.3.** D. P. Raymer. *Aircraft Design: A Conceptual Approach*. AIAA Education Series, 1989

**Ref.2.4.** B. Etkin and L. D. Reid. *Dynamics of Flight: Stability and Control*. John Wiley and Sons, New York, NY, third edition, 1996.

# Appendix C: Supplemental Drawings